

We really appreciate the editor and the reviewer #2 for their thoughtful comments on this manuscript, which was further revised in the new version.

Response to Reviewer #2

I thank the authors for considering my comments. However, I still find myself in disagreement with the conclusion regarding aerosol acidity. The stated intent of section 3.2.3 is to evaluate acidity because of its relevance to health impacts. However, as conceded by the authors, any observation of an apparently acidic aerosol is at odds with the observation of ammonium nitrate being present. To summarise the points raised by myself and the authors, the three possibilities of reconciling these observations are:

- 1. Inaccurate calibration data*
- 2. A high metal cation content*
- 3. Nitrate partitioning into dilute aqueous droplets at high humidities*

Personally, I still find possibility 1 to be highly plausible. While the instrument was cross-calibrated with a HRAMS, this still only makes it as accurate as the HRAMS calibration, which having read the corresponding paper, I have the exact same concerns about. Possibility 2 could also be plausible because the ACSM does not quantify potassium, although if this was the case, I would expect the deviations from perceived neutrality to correlate with a marker for biofuel or coal burning (this could be done by colouring figure R5 with an appropriate marker, e.g. m60).

Possibility 3, on the other hand, I do not find at all plausible in view of figure R5. As far as I can tell, there is no dependency between relative humidity and apparent acidity except for the fact that the RH tends to be low when loadings are low, but this is probably an aspect of the meteorology and not a causal relationship. The apparent agreement noted at low concentrations is within the scatter of the points, which can easily be explained by the low signal-to-noise ratio of the ammonium measurement or possibly the influence of organic acids, which aren't included in the calculation. While there are points with a low NH_4meas/NH_4pred on figure R5b that correspond to RHs approaching 100%, there are also points on the exact same fit line that also correspond to RHs as low as 50%. At these relative humidities, the water content of particles is very low and this causes nitrate to partition to nitric acid in the event of an imbalance (this can be shown using e-AIM, <http://www.aim.env.uea.ac.uk/aim/model3/model3b.php>). In short, if possibility 3 were to be occurring, I would expect the behaviour to vary between 50% and 100%, but this simply isn't the case, according to figure R5b.

To return to the original point, if it is either possibility 1 or 2 that is occurring, then the logical conclusion would be that the ACSM (as operated here) is not a reliable measure of particle acidity. In this context, the NH_4meas vs NH_4pred is only really useful as a technical instrument diagnostic and as such, I still don't see the conclusion that the particles are acidic is supportable.

We really appreciate the reviewer #2 for his/her detailed comments on aerosol

particle acidity. We agree with the reviewer that the discussions on aerosol particle acidity might have large uncertainties. Because the RIE of sulfate was not calibrated for the HR-AMS with pure ammonium sulfate particles, it might be overestimated to a certain degree. We also observed clear K^+ and Na^+ signals in the raw spectra (Figure R1), indicating the presence of these metal ions. In addition, organic acids might be another factor affecting the calculation of aerosol particle acidity. For these uncertainties, we decided to remove the discussions on aerosol particle acidity in the revised manuscript to avoid bringing the wrong messages to the readers.

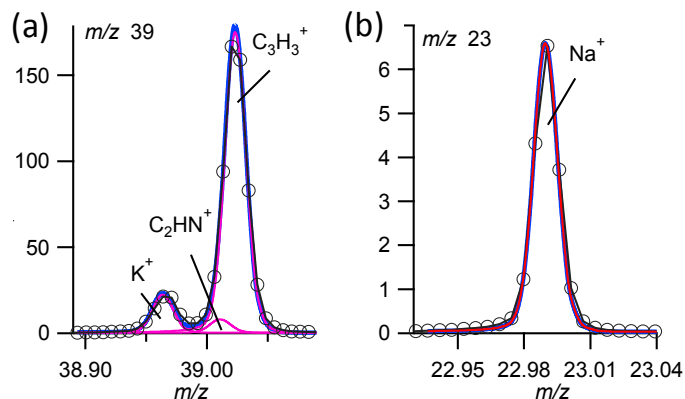


Figure R1. High resolution raw spectra of (a) m/z 39 and (b) m/z 23.

Response to the Editor

From my point of view, the method you applied to predict ammonium and the aerosol acidity might not be completely applicable for the real atmosphere in Beijing. First, all the cations and anions that are likely to be present in a considerable amount in the aerosol salt solution should be included for an ion balance. For example, potassium (as suggested by the referee), calcium, carbonate (or hydrogen carbonate) and organic ions. Second, other ions like carbonate and organic anions tend to make solution basic and neutralize the acidity induced by ammonium cations. You may have to consider these before drawing a conclusion, not mentioned to the data calibration issue.

Thank the editor for your comments. After considering the comments offered by the reviewer#2 and you, we decided to remove the section “3.2.3 Particle acidity” in the revised manuscript unless we have more evidence.

In the last part of Sect. 3.2.1 (Lines 392-400 of version 3), the lower sulfate contribution during APEC has been attributed to the lower RH. In Sect. 3.2.3 (Lines 468-471), however, the reduction of SO_2 is also considered as one reason for the reduction of sulfate. Moreover, what do you mean by lower RH here, the lower aerosol water content or the lower water vapor amount? The two cases would mean different pathways for the oxidation of SO_2 .

RH is positively related to liquid water content. Lower RH is generally associated with lower liquid water content. As a result, aqueous-phase production of sulfate could not be significant during low RH periods. The reduced SO₂ plus the low RH would together decrease the production of sulfate in aqueous-phase. For clarification, we revised the sentence as “The lower sulfate contribution during APEC might be due to the lower RH associated with lower liquid water content, leading to less production of sulfate”.

You have stated that the emission controls during APEC did not significantly affect the regional aerosol bulk composition (do you mean its fraction?) (Line 393-394), but say that you detected a slightly higher reduction of sulfate than other inorganic species (Line 469-470). This seems to be in self-conflict.

Yes, the bulk composition here means the mass fractions of aerosol species. As indicated in Fig. 6, the aerosol bulk composition had changes during APEC, but not significant. Therefore it is not conflict with the description of “a slightly higher reduction of sulfate than other inorganic species”. Such descriptions were removed from the manuscript with the section “3.2.3 Particle acidity”.

22 **Abstract**

23 The megacity of Beijing has experienced frequent severe fine particle pollution during
24 the last decade. Although the sources and formation mechanisms of aerosol particles
25 have been extensively investigated on the basis of ground measurements, real-time
26 characterization of aerosol particle composition and sources above the urban canopy
27 in Beijing is rare. In this study, we conducted real-time measurements of
28 non-refractory submicron aerosol (NR-PM₁) composition at 260 m at the ~~325 m~~
29 Beijing 325 m Meteorological Tower (BMT) from October 10 to November 12, 2014,
30 by using an aerosol chemical speciation monitor (ACSM) along with synchronous
31 measurements of size-resolved NR-PM₁ composition at near ground level using a
32 High-Resolution Time-of-Flight Aerosol Mass Spectrometer (HR-ToF-AMS). The
33 NR-PM₁ composition above the urban canopy was dominated by organics (46%),
34 followed by nitrate (27%) and sulfate (13%). The high contribution of nitrate and high
35 NO₃⁻/SO₄²⁻ mass ratios illustrate an important role of nitrate in particulate matter (PM)
36 pollution during the study period. The organic aerosol (OA) was mainly composed by
37 secondary OA (SOA), accounting for 61% on an average. Different from that
38 measured at the ground site, primary OA (POA) correlated moderately with SOA,
39 likely suggesting a high contribution from regional transport above the urban canopy.
40 The Asia-Pacific Economic Cooperation (APEC) summit with strict emission
41 controls provides a unique opportunity to study the impacts of emission controls on
42 aerosol chemistry. All aerosol species were shown to have significant decreases of
43 40–80% during APEC from those measured before APEC, suggesting that emission
44 controls over regional scales substantially reduced PM levels. However, the bulk
45 aerosol composition was relatively similar before and during APEC as a result of
46 synergetic controls of aerosol precursors. In addition to emission controls, the routine
47 circulations of mountain-valley breezes were also found to play an important role in
48 alleviating PM levels and achieving the “APEC blue” effect. The evolution of vertical
49 differences between 260 m and the ground level was also investigated. Our results
50 show complex vertical differences during the formation and evolution of severe haze
51 episodes that are closely related to aerosol sources and boundary layer dynamics.

52 **1 Introduction**

53 Beijing (39°56'N, 116°20' E), the capital of China, is one of the largest megacities
54 in the world with more than 21 million residents and 5.4 million vehicles in operation
55 by the end of 2013 (Beijing Municipal Bureau of Statistics, 2014). In the west, north,
56 and northeast, the city is surrounded by the Taihang and Yanshan mountains at
57 approximately 1000–1500 m above sea level. The fan-shaped topography in addition
58 to the rapid urbanization has caused frequent severe haze pollution episodes in Beijing.
59 These conditions have received a significant amount of attention from atmospheric
60 scientists, the government, and the general public (Sun et al., 2006;Sun et al.,
61 2012a;Sun et al., 2013c;Guo et al., 2014;Sun et al., 2014). For in-depth elucidation of
62 severe urban haze formation and particulate matter (PM) characteristics, extensive
63 studies have been conducted in Beijing including real-time online measurements and
64 filter sampling with subsequent offline analyses (Sun et al., 2006;Pope III et al.,
65 2009;Zhao et al., 2013). Aerosol Mass Spectrometers (AMS), which are capable of
66 determining size-resolved aerosol compositions with high sensitivity, have been
67 widely deployed in Beijing and other cities in China since 2006 (Huang et al.,
68 2012b;Zhang et al., 2014;Li et al., 2015). Numerous conclusions and findings have
69 been obtained since then, which have greatly improved our understanding of aerosol
70 composition, formation mechanisms, and evolution processes (Sun et al., 2010;Xiao
71 et al., 2011;Zhang et al., 2012;Hu et al., 2013;Huang et al., 2013;Guo et al.,
72 2014;Zhang et al., 2014;Li et al., 2015). However, most previous AMS studies include
73 short-term measurements, of generally less than two months, because of the high cost
74 and maintenance of the instrument. The recently developed aerodyne aerosol chemical
75 speciation Monitor (ACSM) (Ng et al., 2011) has been used in some studies for
76 examining the chemical composition, sources, and processes of atmospheric aerosols
77 in China. The advantage of the ACSM is its robustness for real-time long-term
78 measurements of aerosol particle composition with little attendance (Ng et al.,
79 2011;Sun et al., 2012a;Sun et al., 2013c;Budisulistiorini et al., 2014;Sun et al.,
80 2014;Jiang et al., 2015; Parworth et al., 2015;Petit et al., 2015). The first ACSM
81 measurements in Beijing highlighted the important role of nitrate in PM pollution in

82 summer, which was mainly attributed to the partitioning of nitric acid into liquid
83 ammonium nitrate particles (Sun et al., 2012a). The PM pollution characteristics also
84 dramatically differed between summer and winter. Agricultural burning and
85 photochemical production play major roles in PM pollution in summer (Li et al.,
86 2010;Huang et al., 2012a;Sun et al., 2012a;Zhang et al., 2015), whereas coal
87 combustion is the dominant source of PM in winter (Sun et al., 2013c). A more
88 detailed analysis of a severe haze pollution episode occurred in January 2013
89 suggested that stagnant meteorological conditions, source emissions, secondary
90 production and regional transport are four major factors driving the formation and
91 evolution of haze pollution in Beijing during winter (Sun et al., 2013c;Guo et al.,
92 2014;Sun et al., 2014;Zhang et al., 2014).

93 Despite extensive efforts for the characterization of fine particle pollution in
94 Beijing, most studies are conducted at ground sites, which are subject to significant
95 influences of local emission sources such as traffic, cooking, and biomass burning. In
96 comparison, measurements obtained above the urban canopy with much less influence
97 of local source are more representative for a large scale, which is of great importance
98 for characterizing regional transport. However, such studies in Beijing are rare due to
99 the absence of high platforms. The ~~325 m~~ Beijing 325 m Meteorological Tower (BMT)
100 is a unique platform for measuring aerosol and gaseous species at various heights in
101 Beijing megacity. Moreover, this platform is beneficial for studying the interactions of
102 the lower boundary layer (<300 m) and air pollution, particularly during autumn and
103 winter when the nocturnal planetary boundary height is often below 300 m (Ting et al.,
104 2008;Zhang et al., 2013). Based on the BMT measurements, Sun et al. (2009;2013a)
105 reported that the SO₂ concentration reached its maximal value at 50 m during heating
106 periods, whereas PM_{2.5} showed a “higher top and lower bottom” vertical pattern due
107 to the inversions of temperature (*T*) and relative humidity (RH) during summer hazy
108 days. Guinot et al. (2006) and Meng et al. (2008) also determined that local
109 concentration peaks at 50 m to 100 m were likely related to the urban canopy.
110 However, real-time characterization of aerosol particle composition above the urban
111 canopy has been performed only once (Sun et al., 2015). The two-week study found

112 substantially different aerosol compositions between ground level and 260 m. In
113 addition, the compositional differences at the two heights were found to be strongly
114 associated with source emissions, the vertical mixing mechanism, and
115 RH/T-dependent secondary production. Because these measurements only lasted two
116 weeks, the aerosol characteristics and sources above the urban canopy remain poorly
117 understood.

118 The 2014 Asia–Pacific Economic Cooperation (APEC) summit was hosted in
119 Beijing during November 5–11, 2014, when strict emission control measures were
120 implemented in Beijing and surrounding regions to ensure the air quality. During
121 November 3–12, emission controls such as reducing the number of vehicles in
122 operation by approximately 50%, shutting down factories, stopping construction
123 activities, and enhancing the cleanliness of urban roads were gradually implemented
124 (<http://www.bjepb.gov.cn/bjepb/323474/331443/331937/333896/412827/index.html>,
125 in Chinese). The neighboring provinces such as Hebei, Tianjin, and Shandong
126 implemented the same emission controls during APEC
127 (<http://www.bjepb.gov.cn/bjepb/324122/412670/index.html>, in Chinese). As a result,
128 the PM levels in Beijing during the summit were significantly reduced, leading to
129 “APEC blue,” a phrase commonly used to refer to the good air quality. However, the
130 response of aerosol chemistry to emission controls over a regional scale has not been
131 investigated. Measurements above the urban canopy are ideal for evaluating the roles
132 of emission controls in reducing PM levels under the condition of minimizing the
133 influences of local point sources.

134 In this study, we conduct real-time measurements of non-refractory submicron
135 aerosol (NR-PM₁) composition including organics (Org), sulfate (SO₄²⁻), nitrate
136 (NO₃⁻), ammonium (NH₄⁺), and chloride (Cl⁻) at 260 m at the BMT before and during
137 APEC, October 10–November 2 and November 3–12, 2014, respectively, by using an
138 ACSM. The aerosol composition, diurnal variation, and sources above the urban
139 canopy are investigated in detail. The responses of aerosol composition, particle
140 acidity, and sources of organic aerosol (OA) to emission controls are elucidated by
141 comparing the changes before and during APEC, and the roles of meteorological

142 conditions in PM reduction during APEC are discussed. In addition, the vertical
143 differences of aerosol composition and its interactions with boundary layer dynamics
144 are also examined.

145

146 **2 Experimental methods**

147 **2.1 Sampling site and measurements**

148 All of the measurements in this study were conducted at the same site as that
149 reported by Sun et al. (2013c), which is an urban site at the Institute of Atmospheric
150 Physics, Chinese Academy of Sciences, between North 3rd and 4th Ring Road from
151 October 10 to 12 November, 2014. The ACSM and gas measurement instruments
152 were mounted inside a container at 260 m on the BMT. The ACSM sampling setup
153 used in this study is similar to that described by Sun et al. (2012a). Briefly, aerosol
154 particles were first sampled into the container with a PM_{2.5} cyclone to remove coarse
155 particles larger than 2.5 μm . After passing through a diffusion silica-gel dryer, aerosol
156 particles were sampled into the ACSM at a flow rate of ~ 0.1 L/min. The ACSM was
157 operated by alternating ambient air and filtered air with a mass spectrometer at a
158 scanning rate of 500 ms amu^{-1} from m/z 10 to 150. The data were saved every two
159 cycles, leading to a time resolution of approximately 5 min. The detailed principles of
160 the ACSM can be found elsewhere (Ng et al., 2011; Sun et al., 2012a). An Aerodyne
161 High-Resolution Time-of-Flight AMS (HR-ToF-AMS) was simultaneously deployed
162 near the ground level at the same location to measure the size-resolved NR-PM₁
163 aerosol composition. Details of the sampling and operation procedures of the
164 HR-ToF-AMS was given in Xu et al. (2015).

165 Meteorological variables including wind speed (WS), wind direction (WD), RH,
166 and T at 15 heights of 8, 15, 32, 47, 65, 100, 120, 140, 160, 180, 200, 280, and 320 m
167 were obtained from the BMT. In addition, a Doppler wind lidar (Windcube 200,
168 Leosphere, Orsay, France) was deployed at the same location to obtain the wind
169 profiles from 100 m to 5000 m with a spatial resolution of 50 m and a time resolution
170 of 10 min. All of the data in this study are reported in Beijing Standard Time (BST),
171 which equals Coordinated Universal Time (UTC) plus 8 h.

172 2.2 Data analysis

173 The ACSM data were analyzed for the mass concentration and chemical
174 composition of NR-PM₁ species including organics, sulfate, nitrate, ammonium, and
175 chloride by using ACSM standard data analysis software (v. 1.5.3.0). Detailed
176 analytical procedures have been reported by Ng et.al (2011) and Sun et.al (2012a).
177 Similar to that in previous studies in Beijing (Sun et al., 2011; Sun et al., 2012a; Sun et
178 al., 2013c; Sun et al., 2014), an empirical and constant collection efficiency (CE) of
179 0.5 was applied during the entire campaign to compensate for the particle loss due
180 mainly to particle bounce at the vaporizer (Matthew et al., 2008). The CE of 0.5 is
181 rationale for this study because aerosol particles were dried, and the mass fraction of
182 ammonium nitrate was overall below the threshold value (40%) that affects CE
183 (Middlebrook et al., 2012). The average ratio of measured NH₄⁺ (NH₄⁺_{meas}) versus
184 predicted NH₄⁺ (NH₄⁺_{pred}) was 0.56, suggesting that the aerosol particles were acidic.
185 Although the particle acidity would have a slightly higher CE than 0.5 (~0.59) if the
186 equation $CE_{dry} = \max(0.45, 1.0 - 0.73 \times (NH_4^+_{meas}/NH_4^+_{pred}))$ recommended by
187 Middlebrook et al. (2012) were used, no effect on CE is present if using the
188 parameterization reported by Quinn et al. (2006). For consistency with our previous
189 studies and with the HR-ToF-AMS measurements at the ground site, we maintained
190 CE = 0.5 in this study. The default relative ionization efficiency (RIE) values, 1.4 for
191 organics, 1.1 for nitrate, 1.2 for sulfate, and 1.3 for chloride except ammonium (6.5)
192 which was determined from pure ammonium nitrate particles. Note that the ACSM
193 measurements were compared with those of HR-AMS at the same location before the
194 campaign. All submicron aerosol species measured by the ACSM were highly
195 correlated with those by the HR-AMS ($r^2 > 0.97$). Although the total NR-PM₁ mass
196 measured by the ACSM agreed well with that by HR-AMS ($r^2 = 0.99$, slope = 0.99),
197 the regression slopes of ACSM against HR-AMS varied from 0.61–1.24 for different
198 aerosol species. Because ACSM was found to have a larger uncertainty in
199 quantification of submicron aerosol species, particularly in determination of relative
200 ionization efficiency, the mass concentrations of aerosol species measured by the
201 ACSM at 260 m were further corrected using the regression slopes of

202 ACSM/HR-AMS obtained from the inter-comparison study.

203 Positive matrix factorization (PMF) with the PMF2.exe algorithm (Paatero and
204 Tapper, 1994) was performed on the ACSM OA mass spectra to resolve potential OA
205 components with different sources and processes. Only m/z 's < 125 was included in
206 the PMF analysis due to the large interferences of naphthalene signals on several
207 larger m/z 's (e.g., m/z 127–129) (Sun et al., 2012a; Sun et al., 2013c; Sun et al., 2014).
208 The PMF results were then evaluated by using an Igor Pro-based PMF Evaluation
209 Tool (PET, v 2.06) (Ulbrich et al., 2009) with following procedures detailed by Zhang
210 et al. (2011). After careful evaluation of the mass spectra and time series of OA
211 factors, a two-factor solution, i.e., an oxygenated OA (OOA) and a hydrocarbon-like
212 OA (HOA) with $f_{\text{peak}} = 0.4$, was chosen. A more detailed PMF diagnostics is
213 presented in Figs. S1, S2 and Table S1. While the 3-factor solution resolved an
214 unrealistic factor with unexpectedly high m/z 12 and m/z 15, the 2-factor solution at
215 $f_{\text{peak}} = 0$ showed much higher m/z 44 in HOA spectrum, which is generally a
216 characteristics of OOA (Fig. S3).

217 **2.3 Air mass trajectory analyses**

218 The three-day (72 h) back trajectories were calculated every hour at 500 m height
219 using the Hybrid Single-Particle Lagrangian Integrated Trajectory (HYSPPLIT, NOAA)
220 4.9 model (Draxler and Hess, 1997; Li et al., 2015). The trajectories were then
221 grouped into four clusters before and during APEC using the algorithm of cluster
222 analysis. The clustering of trajectories is based on the total spatial variance (TSV)
223 method (Draxler et al., 2012). This method minimizes the inter-cluster differences
224 among trajectories while maximizing the inter-cluster differences, which has been
225 widely used in previous studies (Sun et al., 2014; Zhang et al., 2014; Li et al., 2015)

226 **3 Results and discussion**

227 **3.1 General description**

228 **3.1.1 Submicron aerosol and meteorology**

229 The NR-PM₁ mass concentration varied significantly from 0.7 to 254 $\mu\text{g m}^{-3}$,
230 with an average of 53.5 $\mu\text{g m}^{-3}$. As indicated in Fig. 1, the variations of NR-PM₁ were
231 strongly associated with WD and WS. The formation of severe haze episodes was

232 generally initiated by a WD change from northerly to southerly and a decrease of WS
233 to less than 5 m s^{-1} below 1 km. The southern air flow and low WS were then
234 dominant most of the time during the evolution of haze episode; subsequently, the air
235 masses changed from the south to the north/northwest, leading to a rapid decrease of
236 PM level in a few hours. Haze episodes with such life cycle driven by meteorological
237 conditions have also been observed many times in Beijing (Jia et al., 2008; Sun et al.,
238 2013c; Guo et al., 2014; Sun et al., 2014). Note that a mountain–valley breeze lasting
239 approximately half a day was frequently observed throughout the study, which
240 reduced the daytime PM levels to a certain degree. As shown in Fig. 1, most of the
241 cleaning processes were similar, all driven by the switch of air masses from
242 south/southwest to north/northwest associated with high WS across the entire vertical
243 layer ($>5 \text{ m s}^{-1}$). However, the cleaning process occurring on October 20–21 was
244 different. As the WD changed from the south to the northwest/northeast, the NR-PM₁
245 concentration remained high. This phenomenon can be explained by the low WS (<4
246 m s^{-1}) below 500 m and the high RH (Figs. 2, S4). The NR-PM₁ began to decrease at
247 ~20:00 as WD shifted to the south associated with a decrease in RH. This result
248 indicates that a cleaner and dryer air mass was located to the south of Beijing during
249 this stage. Such a cleaning process by southern air flow is not common and is
250 generally weaker than that by northern/northwestern flow. This observation is
251 supported by the higher NR-PM₁ concentration of $\sim 20 \mu\text{g m}^{-3}$ on October 21 than
252 during other cleaning periods at $\sim <5 \mu\text{g m}^{-3}$. The average mass concentration of
253 NR-PM₁ during APEC was $24.1 \mu\text{g m}^{-3}$, which is significantly lower than the $65.1 \mu\text{g}$
254 m^{-3} recorded before APEC, indicating a large reduction of PM during APEC. In
255 addition, the southern air mass occurred less frequently and had a shorter duration
256 during APEC. These results manifest that meteorology in addition to emission
257 controls might have played an important role in reducing PM levels during APEC.

258 The NR-PM₁ species showed similar and dramatic variations to the total NR-PM₁
259 mass (Fig. 2). In particular, three haze episodes before APEC (Ep1, Ep2, and Ep3 in
260 Fig. 2d) and two episodes during the summit (APEC1 and APEC2 in Fig. 2d) were
261 observed in this study. The three episodes before APEC were all characterized by high

262 RH at 48–70% and low WS at 2.3–3.4 m s⁻¹, elucidating the important roles of
263 stagnant meteorological conditions in severe haze formation. In comparison, the RH
264 in the two episodes during APEC was lower at 34–38%, and the WS was comparably
265 higher at 3.1–3.8 m s⁻¹ (Table 1). These results suggest that the meteorological
266 conditions during APEC appeared to be more favorable for dispersion of pollutants.
267 Indeed, clear accumulation processes of aerosol species were observed for three
268 episodes before APEC, yet they were much weaker during the summit. However, the
269 two episodes during APEC showed obvious temperature inversions, which inhibited
270 the vertical convection of pollutants. The meteorological conditions during haze
271 episodes differed substantially from those during clean periods, which were
272 characterized by high WS at >5 m s⁻¹ and low RH at <20%.

273 The NR-PM₁ was dominated by organics, accounting for on average 46% of the
274 total mass, followed by nitrate at 27%, sulfate at 13%, ammonium at 9%, and chloride
275 at 5%. The nitrate contribution ranged from 27% to 28% during the three episodes
276 before APEC and from 29% to 31% in the two episodes during APEC, which is
277 significantly higher than the sulfate contribution of 10–15% and 8–11%, respectively
278 (Fig. 6). Although the dominance of organics in PM₁ was consistent with that in
279 previous studies in Beijing (Sun et al., 2012a; Sun et al., 2013c; Guo et al., 2014; Sun et
280 al., 2014; Zhang et al., 2014), the nitrate contribution in this study was approximately
281 twice that of sulfate and significantly higher than previously reported values of 16%
282 in 2011 (Sun et al., 2013c) and 13–14% in 2013 (Sun et al., 2014; Zhang et al., 2014).
283 The mass ratio of NO₃⁻/SO₄²⁻ can be used to indicate the relative importance of
284 mobile and stationary sources (Arimoto et al., 1996). Therefore, higher NO₃⁻/SO₄²⁻ in
285 this study likely indicates the predominance of mobile source rather than stationary
286 source. Because the continuous increase of NO_x emissions associated with a decrease
287 in SO₂ (Wang et al., 2013), nitrate is expected to play a more important role in PM
288 pollution in the future. Our results highlight that NO_x emission control should be a
289 priority in mitigating air pollution, particularly in non-heating seasons with low SO₂
290 precursors.

291 Figure 3 further shows the time series of NO₃⁻/SO₄²⁻ mass ratio and sulfur

292 oxidation ratio (SOR) calculated as the molar fraction of sulfate in total sulfur (i.e.,
293 sulfate and SO₂) (Sun et al., 2014). The NO₃⁻/SO₄²⁻ was ubiquitously greater than 1
294 during five haze episodes, indicating the importance of nitrate in the formation of
295 severe haze pollution. Interestingly, we observed a rapid increase in NO₃⁻/SO₄²⁻
296 during the formation stage of a pollution episode followed by a decrease in
297 NO₃⁻/SO₄²⁻ during the subsequent evolution stage. The variations of NO₃⁻/SO₄²⁻
298 illustrate that two different formation mechanisms might drive the formation and
299 evolution of haze episodes. During the early stage of haze formation, the RH was
300 relatively low and the formation rate of sulfate was correspondingly low, which is
301 supported by the low SOR values. Consequently, the nitrate formation played a
302 dominant role during this stage. The SO₄²⁻ concentration remained consistently low
303 when the nitrate began to increase (Fig. 2d). As the RH continued to increase, the
304 SOR showed a corresponding increase indicating that more SO₂ was oxidized to form
305 sulfate, most likely via aqueous-phase processing (Zhang and Tie, 2011; Sun et al.,
306 2013b). The SO₄²⁻ concentration then showed a substantial increase, and the
307 NO₃⁻/SO₄²⁻ ratio decreased as a result. For example, during Ep2, the hourly
308 NO₃⁻/SO₄²⁻ increased from ~1.1 to 4.0 during the formation stage and then decreased
309 to ~1.8 during the evolution stage. These results indicate that SO₄²⁻ played an
310 enhanced role in PM pollution during the evolution stage of haze episodes with high
311 RH. Moreover, the NO₃⁻/SO₄²⁻ ratios during clean periods (~0.3) were much lower
312 than those during haze episodes. One explanation is that the nitrate in clean air masses
313 from north/northwest is significantly lower than that of sulfate.

314 **3.1.2 Sources and composition of OA**

315 Two OA factors, HOA and OOA, were identified in this study. The HOA
316 spectrum was similar to those determined at other urban sites (Huang et al.,
317 2012a; Sun et al., 2012a; Sun et al., 2012b), which is characterized by prominent
318 hydrocarbon ion peaks of *m/z* 27, 29, 41, 43, 55, 57 (Fig. 4a). The HOA spectrum
319 showed a higher *m/z* 55/57 ratio compared with that of exhaust aerosols from diesel
320 trucks and gasoline vehicles (Mohr et al., 2009), yet it had characteristics similar to
321 those resolved in urban Beijing (Sun et al., 2010; Sun et al., 2012a). The high *m/z*

322 55/57 ratio and the two visible peaks at meal times in diurnal variations (Fig. 4b)
323 indicate the impact of local cooking activities (Sun et al., 2011; Sun et al., 2012a; Sun
324 et al., 2013c). However, the two HOA peaks were much smaller than those observed
325 at the ground site (Xu et al., [in preparation 2015](#)), indicating a significantly smaller
326 impact of local cooking emissions on OA at 260 m. Moreover, the HOA spectrum
327 showed a considerable m/z 60 peak, a marker m/z for biomass burning (Aiken et al.,
328 2009; Huang et al., 2011; Zhang et al., 2015). The fraction of m/z 60 was 0.9%, which
329 is much higher than ~0.3% in the absence of biomass burning. All these results
330 suggest that HOA was a primary OA factor combined with traffic, cooking, and
331 biomass burning emissions. Limited by the ACSM spectra and PMF analysis, we were
332 not able to separate the different primary OA factors in this study. HOA correlated
333 well with chloride ($r^2 = 0.61$) and moderately well with secondary inorganic species
334 ($r^2 = 0.42$ – 0.65), indicating that a major fraction of HOA shared similar sources to
335 secondary species at 260 m, which was likely from regional transport. HOA on
336 average contributed 39% of total organics, which is less than the 57% observed at the
337 ground site during the same study period (Xu et al., [in preparation 2015](#)). This result
338 indicates a smaller impact of primary sources above the urban canopy. The diurnal
339 cycle of HOA was relatively flat with two visible peaks occurring at noon and night.
340 The HOA contribution to OA was relatively constant throughout the day, ranging from
341 36% to 43%. This result further supports the theory that HOA above the urban canopy
342 was dominantly from regional transport and was well mixed with regional secondary
343 OA (SOA). Indeed, the correlation of HOA with OOA in this study was quite high (r^2
344 = 0.76), supporting that HOA and OOA might have some common sources (e.g.,
345 regional transport) at 260 m.

346 The mass spectrum of OOA resembles that identified in 2012 in summer in
347 Beijing (Sun et al., 2012a) in addition to those resolved at other urban sites (Ulbrich et
348 al., 2009), which is characterized by a prominent m/z 44 peak (mainly CO_2^+). OOA
349 dominated the OA composition throughout the day, ranging from 57% to 64%. The
350 average OOA contribution to OA was 61%, which is close to those previously
351 reported in Beijing (Huang et al., 2010; Sun et al., 2012a; Sun et al., 2013c). The

352 diurnal cycle of OOA was relatively flat, yet a gradual increase during the day was
353 also observed despite the rising planetary boundary layer, suggesting daytime
354 photochemical processing. OOA is often considered as a good surrogate of SOA
355 (Zhang et al., 2005;Jimenez et al., 2009;Ng et al., 2011). In this study, OOA tracked
356 well with secondary inorganic species such as NO_3^- , SO_4^{2-} ($r^2 = 0.72\text{--}0.90$), which is
357 consistent with previous conclusions that OOA is a secondary species in nature
358 (Zhang et al., 2005;Sun et al., 2012a).

359 **3.2 Response of aerosol chemistry to emission controls**

360 **3.2.1 Aerosol composition**

361 Figure 5 shows the variations of aerosol composition as a function of NR-PM₁
362 mass loading before and during APEC. The organics contribution showed a notable
363 decrease from 62% to 32% as the NR-PM₁ mass concentration increased from <10 μg
364 m^{-3} to >200 $\mu\text{g m}^{-3}$ before APEC. In contrast, the sulfate contribution showed a
365 corresponding increase from 8% to 22%. Except for low values at NR-PM₁ <10 μg
366 m^{-3} , nitrate and ammonium constituted relatively constant fractions of NR-PM₁ across
367 different NR-PM₁ loadings and varied at 21–31% and 8–12%, respectively. These
368 results highlighted the enhanced roles of secondary inorganic species in severe PM
369 pollution before APEC. This observation is further supported by a comparison of
370 average chemical composition between three pollution episodes and a clean event (Fig.
371 6). The secondary inorganic aerosol ($\text{SIA} = \text{SO}_4^{2-} + \text{NO}_3^- + \text{NH}_4^+$) on average
372 contributed 46–51% of the total NR-PM₁ mass during the three episodes before APEC,
373 which is significantly higher than the 40% reported during the clean event (Fig. 6).
374 The NR-PM₁ mass loading-dependent aerosol composition showed a different
375 behavior during APEC. As shown in Fig. 5b, all aerosol species had relatively
376 constant contributions to NR-PM₁ at 10–100 $\mu\text{g m}^{-3}$. The contribution of organics
377 ranged from 43% to 58%, which is overall higher than those before APEC. This result
378 indicates an enhanced role of organics during APEC, particularly during severe PM
379 pollution periods. Similarly, nitrate contributed the largest fraction of NR-PM₁,
380 varying from 23% to 32%. Figure 5 also shows a very broad range of NR-PM₁ mass
381 concentration with the maximum concentration over 200 $\mu\text{g m}^{-3}$ before APEC. In

382 contrast, the range of NR-PM₁ was much narrower during APEC, suggesting a
383 significantly lower amount of severe haze pollution during APEC. Indeed, 93% of the
384 time during APEC, the NR-PM₁ level was lower than 60 μg m⁻³, whereas 49% of the
385 time before APEC exceeded such a concentration level. These results indicate that the
386 air pollution was substantially more severe before APEC. The average mass
387 concentration of NR-PM₁ was 24.1 μg m⁻³ during APEC, which is 63% lower than
388 the 65.1 μg m⁻³ recorded before APEC (Fig. 6). This result demonstrates a significant
389 reduction of PM during APEC due to emission controls and better weather conditions
390 including higher WS and lower RH. However, the bulk NR-PM₁ composition was
391 rather similar before and during APEC, both of which were dominated by organics, 46%
392 versus 47%, followed by nitrate at 27% versus 29% and sulfate at 14% versus 10%
393 (Fig. 6). The lower sulfate contribution during APEC might be due to the lower RH
394 associated with lower liquid water content, leading to less production of sulfate. These
395 results highlight that the emission controls during APEC did not significantly affect
396 the regional aerosol bulk composition, although the mass concentrations of precursors
397 and aerosol species were reduced substantially. One possible explanation is the
398 synergetic control of various precursors such as SO₂, NO_x, and volatile organic
399 compounds (VOCs) over a regional scale during APEC. Our results clearly imply that
400 synergetic controls of the emissions of precursors over a regional scale are efficient
401 for mitigating air pollution in North China.

402 3.2.2 Diurnal variations

403 The diurnal variations of meteorological variables, NR-PM₁ species, and OA
404 components before and during APEC are presented in Fig. 7. The diurnal cycles of
405 meteorological conditions were overall similar before and during APEC except for
406 lower temperatures and RH during APEC. The WS during APEC was consistently
407 higher than that before APEC, particularly in the morning (04:00–12:00) and evening
408 (18:00–22:00). Although the WD during APEC was dominantly from the northwest at
409 night and shifted to the south during the day, it was mainly from the south before
410 APEC (Fig. 2c).

411 The total NR-PM₁ showed pronounced diurnal variation with two peaks in early

412 afternoon (12:00–14:00) and late evening (20:00–22:00) that were dominantly
413 influenced by organics. By checking the diurnal cycles of the OA factors, we
414 concluded that the two peaks occurring at meal times are mainly attributed to primary
415 emissions such as cooking-related activities and traffic emissions (Allan et al.,
416 2010;Sun et al., 2011;Sun et al., 2012a). Compared with the diurnal cycles of OA
417 previously observed at the ground site in Beijing (Sun et al., 2012a), the two peaks of
418 organics were considerably smaller. This result indicates that local source emissions
419 can be vertically mixed above the urban canopy but at substantially reduced
420 concentrations. Our results also demonstrate that sampling above the urban canopy is
421 less influenced by local source emissions and can be more representative over a
422 regional scale.

423 SIA and OOA showed similar diurnal patterns before and during APEC, all of
424 which were characterized by gradual increases during the day. These results indicate
425 that their diurnal cycles were driven by similar formation mechanisms before and
426 during APEC such as photochemical processing and daytime vertical mixing. Higher
427 concentrations of secondary species were also observed at night, which might have
428 been associated with a shallower boundary layer height (Sun et al., 2012a). It should
429 be noted that all secondary species showed relatively constant background
430 concentrations, indicating that a major fraction was likely from regional transport. SIA
431 and OOA during APEC showed substantial reductions (45–74%) throughout the day
432 compared with those before APEC, indicating that regional emission controls played a
433 significant role in reducing secondary species during APEC, although the lower RH
434 and higher WS were also important. Moreover, a higher reduction percentage was
435 observed between 04:00 and 12:00, when higher mountain–valley breezes occurring
436 routinely during APEC cleaned the air pollutants more efficiently.

437 The diurnal cycles of chloride showed some differences before and during APEC.
438 Although it was relatively flat during APEC, chloride showed a clear decrease in the
439 afternoon before APEC, likely due to the evaporative loss and dilution effects
440 associated with higher T and the elevated boundary layer (Sun et al., 2012a). The
441 diurnal cycle of HOA showed overall lower concentration during the day except for a

442 pronounced noon peak before and during APEC. Considering that the peak time
443 corresponds to lunch time, we concluded that it was attributed mainly to local cooking
444 sources. In addition, a more significant reduction in evening peak of HOA was
445 observed during APEC. One explanation is that controls of heavy-duty vehicles (HDV)
446 and heavy-duty diesel trucks (HDDT) decreased the HOA emissions at night during
447 APEC.

448 **3.2.3 Particle acidity**

449 ~~Particle acidity is a key parameter that influences aerosol toxicity, hygroscopic~~
450 ~~growth, and heterogeneous reactions (Sun et al., 2010). In this study, we evaluated~~
451 ~~aerosol particle acidity by using the ratio of measured NH_4^+ ($\text{NH}_4^+_{\text{meas}}$) to predicted~~
452 ~~NH_4^+ ($\text{NH}_4^+_{\text{pred}}$), which requires full neutralization of SO_4^{2-} , NO_3^- , and Cl^- : $\text{NH}_4^+_{\text{pred}}$~~
453 ~~$= 18 \times (2 \times \text{SO}_4^{2-}/96 + \text{NO}_3^-/62 + \text{Cl}^-/35.5)$ (Zhang et al., 2007a). Lower~~
454 ~~$\text{NH}_4^+_{\text{meas}}/\text{NH}_4^+_{\text{pred}}$ indicates greater aerosol particle acidity. As shown in Fig. 8,~~
455 ~~$\text{NH}_4^+_{\text{meas}}$ strongly correlated with $\text{NH}_4^+_{\text{pred}}$ before and during APEC ($r^2 = 0.95$ and~~
456 ~~0.91 , respectively), with regression slopes of 0.56 and 0.62 , respectively. Slopes less~~
457 ~~than 1 indicate that aerosol particles above the urban canopy were acidic both before~~
458 ~~and during APEC. It should be noted that we might overestimate the particle acidity~~
459 ~~by counting all chloride as NH_4Cl . As indicated by the prominent m/z 60 in HOA~~
460 ~~spectrum, biomass burning could be an important source of primary aerosol at 260 m.~~
461 ~~Considering that chloride from biomass burning emissions could exist in the form of~~
462 ~~KCl , the approach recommended by Zhang et al. (2007a) would overestimate the~~
463 ~~predicted NH_4^+ and hence the aerosol particle acidity. Compared with the ground site~~
464 ~~measurement, $\text{NH}_4^+_{\text{meas}}/\text{NH}_4^+_{\text{pred}} = 0.75$ and 0.80 for the periods before and during~~
465 ~~APEC, respectively, aerosol particles were more acidic above the urban canopy. One~~
466 ~~reason is that the concentration of SO_2 was higher above the urban canopy than that at~~
467 ~~the ground site (Meng et al., 2008). Another possible explanation is that the NH_3 from~~
468 ~~traffic emissions (Li et al., 2006; Meng et al., 2011) can neutralize more secondary~~
469 ~~inorganic aerosol near the ground level. Moreover, we detected a slight decrease in~~
470 ~~particle acidity during APEC, which is consistent with the slightly higher reduction of~~
471 ~~sulfate than other inorganic species. One reason is likely the slightly greater reduction~~

472 ~~of SO₂ than other gaseous precursors during APEC. It is also possible that the lower~~
473 ~~RH during APEC decreased the aqueous phase formation of sulfate and hence~~
474 ~~decreased particle acidity. Overall, the slight change in aerosol particle acidity~~
475 ~~revealed that the joint emission controls appear to have not affected the particle~~
476 ~~acidity significantly over regional scales, which is consistent with the small changes~~
477 ~~in aerosol composition before and during APEC.~~

478 **3.2.4.3 Meteorological effects**

479 Meteorological parameters contribute the largest uncertainties in evaluating the
480 effects of emission controls on PM reduction. Here we compared the variations of
481 aerosol species as a function of RH and WS before and during APEC. At low RH
482 levels (<40%), all aerosol species appeared to increase linearly as a function of RH in
483 both periods at similar rates of increase. Moreover, the mass concentrations of aerosol
484 species were slightly lower during APEC than those before the summit, indicating
485 small reductions in aerosol species during APEC. By checking the air mass
486 trajectories (Fig. S5), we determined that the low RH periods were mainly associated
487 with the air masses from the north/northwest where fewer emission controls were
488 implemented during APEC. This finding explains the small reductions in aerosol
489 species (~22%) during APEC under the same RH conditions. However, the variations
490 in aerosol species showed substantially different behaviors as a function of RH at high
491 RH levels (>40%) before and during APEC. Whereas most aerosol species continued
492 to linearly increase as function of RH before APEC, they remained relatively constant
493 and even showed decreases during APEC. As a result, significant reductions in aerosol
494 species at high RH levels were observed during APEC. The air masses during high
495 RH periods were found to be dominantly from the south/southeast where strict
496 emission controls were implemented such as Hebei, Tianjin, and Shandong provinces.
497 These results clearly indicate that emission controls played a major role in PM
498 reduction during APEC and that the control effects tended to be more efficient under
499 higher RH periods. The primary HOA and chloride showed decreases when the RH
500 was >60%, indicating that humidity has a significantly lower impact on primary
501 aerosols than secondary components at high RH levels.

502 The mass concentrations of aerosol species showed a strong dependence on WS
503 before and during APEC. For example, the total NR-PM₁ mass was decreased by ~80%
504 from ~100 μg m⁻³ to < 20 μg m⁻³ as WS increased to 7 m s⁻¹ before APEC. These
505 results indicate that wind is efficient in cleaning air pollutants in Beijing, which is
506 consistent with previous conclusions (Han et al., 2009; Sun et al., 2013c). In
507 comparison, the decreasing rates of aerosol species as a function of WS were lower
508 during APEC. As a result, aerosol species showed the largest concentration
509 differences before and during APEC in periods with low WS. As indicated by the
510 wind increase plots in Fig. 109, low and high WS were mainly associated with
511 southern/southeastern and northern/northwestern winds, respectively. These results
512 further indicate that larger reductions of aerosol species occurred in Beijing when air
513 masses were from the south.

514 **3.2.5.4 Back trajectory analysis**

515 Figure 110 presents the average chemical composition of NR-PM₁,
516 corresponding to four clusters before and during APEC, determined from the cluster
517 analysis of back trajectories (Draxler and Hess, 1997). The air masses before APEC
518 were predominantly from the south/southeast at 54% of the time (C1 in Fig. 110a),
519 and the aerosol loading was the highest (96.7 μg m⁻³) among the clusters.
520 Comparatively, the northwesterly clusters (C3 and C4 in Fig. 110a) presented
521 significantly lower aerosol loadings at 8.3 μg m⁻³ and 3.5 μg m⁻³, respectively, with
522 fewer frequencies of 14% and 11%, respectively. Such large differences in aerosol
523 loadings between the northerly and southerly air masses are consistent with the spatial
524 distributions of anthropogenic emissions such as SO₂, NO_x, and BC (Zhang et al.,
525 2007b; Lu et al., 2011). Although the areas to the north/northwest of Beijing are
526 relatively clean with low emissions of anthropogenic primary pollutants, the
527 south/southeast regions are characterized by substantially higher emissions. In
528 addition, 21% of the air masses originated from the west and showed moderately high
529 NR-PM₁ mass at 55.4 μg m⁻³. It should be noted that the air masses from the south
530 were often stagnant, as indicated by their shorter trajectories, which played an
531 important role in facilitating the accumulation of pollutants. The aerosol composition

532 varied significantly among four clusters, reflecting the variety in chemical
533 characteristics of aerosol particles from different source regions. The aerosol particle
534 composition from the southeastern and western clusters (C1 and C2) were dominated
535 by nitrate at 27% and 30% and OOA at 26% and 32%, respectively, with considerable
536 contribution from sulfate at 14% and 10%, respectively. These results elucidate the
537 dominant roles of nitrate and OOA in severe PM pollution before APEC, which
538 differs significantly from previous studies reporting that sulfate was generally more
539 prevalent than nitrate (Huang et al., 2014; Sun et al., 2014). These results also
540 highlight a very different pollution characteristic during the late fall season from that
541 in winter. In comparison, the nitrate contributions were significantly lower, at 17%
542 and 8%, in the two northwestern clusters (C3 and C4) associated with an enhanced
543 contribution of sulfate at 19% and 21%, respectively. Moreover, the cleanest cluster
544 (C4) showed a dominant contribution of organics at 64%, indicating the important
545 role of organics during clean periods (Sun et al., 2010; Sun et al., 2013c).

546 The air masses during APEC showed changes, particularly the increases in
547 frequency of two northwestern clusters (C1 and C4), which was 40% of the time
548 compared with 25% before APEC (Fig. 10b). These two clusters showed similar
549 bulk aerosol compositions to those before APEC yet with reductions of the total
550 NR-PM₁ mass loading at nearly 40–50%. The air masses during APEC were
551 dominated by cluster 3 (C3 in Fig. 10b). Although C3 originated from the north of
552 Beijing, it circulated around the south of Beijing including Baoding, a polluted city in
553 Hebei province, before arriving at the sampling site. As a result, C3 presented the
554 highest aerosol mass loading, at 44.0 $\mu\text{g m}^{-3}$, composed primarily of nitrate and OOA
555 at 30% and 29%, respectively. Moreover, cluster 2 (C2 in Fig. 10b), originating from
556 the northwest, showed a similar aerosol composition yet had an ~50% decrease in
557 total mass compared to C3. One explanation is that air masses in C2 passed through
558 the western Beijing, where is relatively cleaner than the southeastern regions. As
559 shown in Fig. 10, similar clusters before and during APEC showed ubiquitous
560 reductions in NR-PM₁ mass during APEC, indicating that emission controls played an
561 important role in PM reduction. Moreover, the decreases in frequency of

562 southern/southeastern air masses during APEC also helped to alleviate the PM level
563 for the entire period, thus achieving the “APEC blue” effect. Emission controls in
564 surrounding regions south of Beijing should be taken as a priority for mitigation of air
565 pollution in Beijing.

566 **3.3 Vertical differences: insights into emission controls and boundary layer** 567 **dynamics**

568 | Figure 12-11 shows a comparison of the time series of NR-PM₁ species between
569 260 m and the ground level for the entire study. All submicron species showed overall
570 similar variations at the two different heights, indicating their relatively similar
571 sources and evolution processes. However, large vertical differences in aerosol
572 composition were also frequently observed, illustrating complex vertical gradients of
573 aerosol species caused by multiple factors such as local emissions, regional transport,
574 and boundary layer dynamics. The average compositional differences before and
575 | during APEC are shown in Fig. 12-3. Although the concentration difference in
576 NR-PM₁ was close before and during APEC at 12.1 μg m⁻³ and 14.1 μg m⁻³,
577 respectively, the composition differed significantly. SIA dominated the compositional
578 difference before APEC, together accounting for 95% of the total NR-PM₁ mass. In
579 comparison, organics and chloride showed minor vertical differences (<5%). These
580 results indicate different sources and formation mechanisms between SIA and organic
581 aerosol. During APEC, the compositional difference was dominated by organics,
582 accounting for 68% on average, and the contributions of SIA were largely reduced at
583 25%. These results suggest that emission controls over regional scales affect the
584 composition differences between ground level and the urban canopy. As discussed in
585 section 3.2 and by Xu et al. (2015), secondary species including SIA and SOA showed
586 significant reductions at both ground level and 260 m during APEC as a result of
587 emission controls. Although primary OA showed similar reductions as those of SOA
588 above the urban canopy, the changes remained small near the ground level. Thus, the
589 largest organic difference during APEC was mainly caused by local primary source
590 emissions.

591 | The vertical differences in aerosol composition also varied largely among

592 | different haze episodes. As indicated in Fig. 112 and Table 1, Ep3 presented the
593 | smallest vertical differences for all aerosol species, indicating a well-mixed layer
594 | below 260 m. The WS was consistently low at $<2.5 \text{ m s}^{-1}$ across the different heights,
595 | and the WD was predominantly from the south during Ep3. Moreover, the vertical
596 | profiles of extinction showed an evident reduction in pollution from $\sim 2 \text{ km}$ to the
597 | ground on October 28, leading to the formation of Ep3 (Fig. S6). Such boundary layer
598 | dynamics would produce a well-mixed layer in the lower atmosphere, leading to
599 | minor chemical differences between the ground level and 260 m.

600 | Comparatively, the vertical evolution of Ep2 differed significantly (Fig. 134a).
601 | The mass concentrations of all aerosol species between the ground level and 260 m
602 | were similar during the formation stage of Ep2, from October 23 to 9:00 October 24.
603 | However, although aerosol species near the ground level showed large increases after
604 | 9:00 on October 24, they remained relatively constant at 260 m, leading to the largest
605 | vertical concentration gradients among five episodes. The average NR-PM₁ at 260 m
606 | was $143.4 \mu\text{g m}^{-3}$, which is 38% lower than that at the ground site. By checking the
607 | vertical profiles of meteorological variables, we observed a clear temperature
608 | inversion between 120 m and 160 m that formed during 0:00–9:00 on October 24.
609 | Such a temperature inversion formed a stable layer below $\sim 200 \text{ m}$ and inhibited the
610 | vertical mixing of air pollutants between the ground and 260 m. In addition, the
611 | stagnant meteorological conditions as indicated by low WS and high RH further
612 | facilitated the accumulation of ground pollution. It should be noted that the
613 | aqueous-phase processing, most likely fog processing under the high RH conditions
614 | (often $> 90\%$) during this stage, also played an important role in the increase of SIA,
615 | particularly sulfate. This finding is also supported by the significant increase of SOR
616 | during this stage (Fig. 3).

617 | The evolution of the severe Ep2 was terminated at approximately 0:00 on October
618 | 26 when the WD changed from south to northwest. Although the mass concentrations
619 | of aerosol species at 260 m began to show rapid decreases at that time, the
620 | concentration at the ground site decreased significantly after 4 hours. The different
621 | cleaning processes between 260 m and the ground level are closely linked to the

622 | vertical profiles of meteorological variables. As indicated in Fig. 134a, a strong
623 temperature inversion below 320 m was observed during the cleaning period, which
624 resulted in a significantly higher WS and lower RH at 260 m than those at ground
625 level. Indeed, both WS and RH showed clear shears during the cleaning period,
626 suggesting a gradual interaction between the northern air mass and boundary pollution
627 from top to bottom. Such an interacting mechanism resulted in a time lag of
628 approximately 4 h in cleaning the pollutants at ground level over that at 260 m.
629 Similar interactions between boundary layer dynamics and aerosol pollution were also
630 observed on November 1, 5, and 11.

631 The evolution of vertical differences during APEC differed from those in three
632 | episodes before APEC. As shown in Fig. 134b, frequent mountain–valley breezes
633 were observed during November 8–11 (APEC2). The northwest mountain–valley
634 breeze began routinely at approximately midnight and dissipated at approximately
635 noon. The NR-PM₁ aerosol species showed direct responses to the mountain–valley
636 breeze, which was characterized by similar routine diurnal cycles. All aerosol species
637 began to decrease at midnight because the cleaning effects of mountain–valley breeze
638 reached minimum concentrations at noon, then increased continuously when the WD
639 changed to south. The mountain–valley breeze also caused a unique diurnal cycle of
640 | vertical differences. As shown in Fig. 134b, aerosol species were well mixed within
641 the lower boundary layer between 12:00 and 16:00, and the concentrations between
642 260 m and the ground level were similar. However, the differences in concentration
643 began to increase when the boundary layer height decreased after sunset at ~18:00,
644 and the differences were maximum at midnight when the NR-PM₁ mass approached
645 100 $\mu\text{g m}^{-3}$. A detailed check of the evolution of aerosol species showed that such
646 vertical differences in NR-PM₁ were caused mainly by organics from local primary
647 | sources (Xu et al., [in preparation2015](#); Fig. 112). These results indicate that local
648 source emissions played a more important role in PM pollution near ground level
649 during APEC. The concentration differences in NR-PM₁ began to decrease with the
650 occurrence of the mountain–valley breeze and reached a minimum at noon. Our
651 results revealed the important role of mountain–valley breeze in affecting the

652 boundary layer structure and reducing the daytime PM levels during APEC. It was
653 estimated that the mountain–valley breeze caused a reduction in NR-PM₁
654 concentration of approximately 50 μg m⁻³ at the ground site during the day on
655 November 10–11 (Fig. 134b). Therefore, our results illustrated that the achievement
656 of “APEC blue” was also due partly to meteorological effects, particularly the
657 mountain–valley breeze, in addition to emission controls.

658 **4 Conclusions**

659 We have presented a detailed characterization of aerosol particle composition and
660 sources above the urban canopy in Beijing from October 10 to November 12, 2014.
661 This study is unique because it examines strict emission controls implemented during
662 the 2014 APEC summit and synchronous real-time measurements of aerosol particle
663 composition at 260 m and that near the ground level obtained by two aerosol mass
664 spectrometers. The NR-PM₁ composition above the urban canopy was dominated by
665 organics at 46%, followed by nitrate at 27% and sulfate at 13%. The high contribution
666 of nitrate and high NO₃⁻/SO₄²⁻ mass ratios illustrate the important role of nitrate in
667 PM pollution during the study period. This result has significant implications that NO_x
668 emission controls should be prioritized for the mitigation of air pollution in Beijing,
669 particularly in non-heating seasons with low SO₂ precursors. The OA above the urban
670 canopy was dominated by OOA at 61% and included HOA at 39%. Different from
671 that at the ground site, HOA correlated moderately with OOA above the urban canopy,
672 indicating similar sources likely through regional transport.

673 With the implementation of emission controls, the mass concentrations of aerosol
674 species were shown to have decreased significantly by 40–80% during APEC,
675 whereas the bulk aerosol composition was relatively similar before and during APEC.
676 Organics were dominant before and during the summit, at 46% versus 47%,
677 respectively, followed by nitrate at 27% versus 29% and sulfate at 14% versus 10%,
678 respectively. Our results suggest that synergetic controls of various precursors such as
679 SO₂, NO_x, and VOCs over a regional scale would not significantly affect regional
680 aerosol bulk composition, although the mass concentrations would be reduced
681 substantially. By linking aerosol compositions and sources to meteorological

682 conditions, we determined that meteorological parameters, particularly
683 mountain–valley breezes, played an important role in suppressing PM growth and
684 hence reducing PM levels during APEC. Our results elucidated that the good air
685 quality in Beijing during APEC was the combined result of emission controls and
686 meteorological effects, with the former playing the dominant role. We further
687 investigated the vertical evolution of aerosol particle composition by comparing the
688 aerosol chemistry between the ground level and 260 m. We observed very complex
689 vertical differences during the formation and evolution of severe haze episodes that
690 were closely related to aerosol sources (local versus regional) and boundary layer
691 dynamics. Although a stable T inversion layer between 120 m and 160 m associated
692 with stagnant meteorology caused higher concentrations of aerosol species at the
693 ground site, the interaction of boundary layer dynamics and aerosol chemistry during
694 the cleaning processes resulted in a lag time of approximately 4 h in cleaning
695 pollutants near the ground level over those occurring above the urban canopy.

696

697 **Acknowledgements**

698 This work was supported by the National Key Project of Basic Research
699 (2014CB447900), the Strategic Priority Research Program (B) of the Chinese
700 Academy of Sciences (XDB05020501), the Key Research Program of the Chinese
701 Academy of Sciences (KJZD-EW-TZ-G06-01-0), and the Special Fund for
702 Environmental Protection Research in the Public Interest (201409001).

703 **References**

- 704 Aiken, A. C., Salcedo, D., Cubison, M. J., Huffman, J. A., DeCarlo, P. F., Ulbrich, I.
705 M., Docherty, K. S., Sueper, D., Kimmel, J. R., Worsnop, D. R., Trimborn, A.,
706 Northway, M., Stone, E. A., Schauer, J. J., Volkamer, R. M., Fortner, E., de Foy, B.,
707 Wang, J., Laskin, A., Shutthanandan, V., Zheng, J., Zhang, R., Gaffney, J., Marley,
708 N. A., Paredes-Miranda, G., Arnott, W. P., Molina, L. T., Sosa, G., and Jimenez, J.
709 L.: Mexico City aerosol analysis during MILAGRO using high resolution aerosol
710 mass spectrometry at the urban supersite (T0) - Part 1: Fine particle composition
711 and organic source apportionment, *Atmos. Chem. Phys.*, **9**, 6633-6653, 2009.
- 712 Allan, J., Williams, P., Morgan, W., Martin, C., Flynn, M., Lee, J., Nemitz, E., Phillips,
713 G., Gallagher, M., and Coe, H.: Contributions from transport, solid fuel burning
714 and cooking to primary organic aerosols in two UK cities, *Atmos. Chem. Phys.*, **10**,
715 647-668, 2010.
- 716 Arimoto, R., Duce, R., Savoie, D., Prospero, J., Talbot, R., Cullen, J., Tomza, U.,
717 Lewis, N., and Ray, B.: Relationships among aerosol constituents from Asia and
718 the North Pacific during PEM - West A, *Journal of Geophysical Research:*
719 *Atmospheres* (1984–2012), **101**, 2011-2023, 1996.
- 720 Budisulistiorini, S., Canagaratna, M., Croteau, P., Baumann, K., Edgerton, E.,
721 Kollman, M., Ng, N., Verma, V., Shaw, S., and Knipping, E.: Intercomparison of an
722 Aerosol Chemical Speciation Monitor (ACSM) with ambient fine aerosol
723 measurements in downtown Atlanta, Georgia, *Atmospheric Measurement*
724 *Techniques*, **7**, 1929-1941, 2014.
- 725 Draxler, R. R., and Hess, G.: Description of the HYSPLIT4 modeling system, *Air*
726 *Resources Laboratory*, Silver Spring, Maryland, 1997.
- 727 Guinot, B., Roger, J.-C., Cachier, H., Pucari, W., Jianhui, B., and Tong, Y.: Impact of
728 vertical atmospheric structure on Beijing aerosol distribution, *Atmos. Environ.*, **40**,
729 5167-5180, 2006.
- 730 Guo, S., Hu, M., Zamora, M. L., Peng, J., Shang, D., Zheng, J., Du, Z., Wu, Z., Shao,
731 M., and Zeng, L.: Elucidating severe urban haze formation in China, *Proc. Natl.*
732 *Acad. Sci. U.S.A.*, **111**, 17373-17378, 2014.
- 733 Han, S., Kondo, Y., Oshima, N., Takegawa, N., Miyazaki, Y., Hu, M., Lin, P., Deng, Z.,
734 Zhao, Y., and Sugimoto, N.: Temporal variations of elemental carbon in Beijing,
735 *Journal of Geophysical Research: Atmospheres* (1984–2012), **114**, D23202,
736 doi:23210.21029/22009JD012027, 2009.
- 737 Hu, W. W., Hu, M., Yuan, B., Jimenez, J. L., Tang, Q., Peng, J., Hu, W., Shao, M.,
738 Wang, M., and Zeng, L.: Insights on organic aerosol aging and the influence of
739 coal combustion at a regional receptor site of central eastern China, *Atmos. Chem.*
740 *Phys.*, **13**, 095, 2013.
- 741 Huang, K., Zhuang, G., Lin, Y., Fu, J., Wang, Q., Liu, T., Zhang, R., Jiang, Y., Deng,
742 C., and Fu, Q.: Typical types and formation mechanisms of haze in an Eastern Asia
743 megacity, Shanghai, *Atmos. Chem. Phys.*, **12**, 105-124, 2012a.
- 744 Huang, R. J., Zhang, Y., Bozzetti, C., Ho, K. F., Cao, J. J., Han, Y., Daellenbach, K. R.,
745 Slowik, J. G., Platt, S. M., Canonaco, F., Zotter, P., Wolf, R., Pieber, S. M., Bruns,
746 E. A., Crippa, M., Ciarelli, G., Piazzalunga, A., Schwikowski, M., Abbaszade, G.,

747 Schnelle-Kreis, J., Zimmermann, R., An, Z., Szidat, S., Baltensperger, U., El
748 Haddad, I., and Prevot, A. S.: High secondary aerosol contribution to particulate
749 pollution during haze events in China, *Nature*, 514, 218-222, 10.1038/nature13774,
750 2014.

751 Huang, X.-F., He, L.-Y., Hu, M., Canagaratna, M., Sun, Y., Zhang, Q., Zhu, T., Xue,
752 L., Zeng, L.-W., and Liu, X.-G.: Highly time-resolved chemical characterization of
753 atmospheric submicron particles during 2008 Beijing Olympic Games using an
754 Aerodyne High-Resolution Aerosol Mass Spectrometer, *Atmos. Chem. Phys.*, 10,
755 8933-8945, 2010.

756 Huang, X.-F., He, L.-Y., Xue, L., Sun, T.-L., Zeng, L.-W., Gong, Z.-H., Hu, M., and
757 Zhu, T.: Highly time-resolved chemical characterization of atmospheric fine
758 particles during 2010 Shanghai World Expo, *Atmos. Chem. Phys.*, 12, 4897-4907,
759 2012b.

760 Huang, X.-F., Xue, L., Tian, X.-D., Shao, W.-W., Sun, T.-L., Gong, Z.-H., Ju, W.-W.,
761 Jiang, B., Hu, M., and He, L.-Y.: Highly time-resolved carbonaceous aerosol
762 characterization in Yangtze River Delta of China: Composition, mixing state and
763 secondary formation, *Atmos. Environ.*, 64, 200-207, 2013.

764 Huang, X. F., He, L. Y., Hu, M., Canagaratna, M. R., Kroll, J. H., Ng, N. L., Zhang, Y.
765 H., Lin, Y., Xue, L., Sun, T. L., Liu, X. G., Shao, M., Jayne, J. T., and Worsnop, D.
766 R.: Characterization of submicron aerosols at a rural site in Pearl River Delta of
767 China using an Aerodyne High-Resolution Aerosol Mass Spectrometer, *Atmos.*
768 *Chem. Phys.*, 11, 1865-1877, 10.5194/acp-11-1865-2011, 2011.

769 Jia, Y., Rahn, K. A., He, K., Wen, T., and Wang, Y.: A novel technique for quantifying
770 the regional component of urban aerosol solely from its sawtooth cycles, *J.*
771 *Geophys. Res.*, 113, D21309, 10.1029/2008jd010389, 2008.

772 Jiang, Q., Sun, Y. L., Wang, Z., and Yin, Y.: Aerosol composition and sources during
773 the Chinese Spring Festival: fireworks, secondary aerosol, and holiday effects,
774 *Atmos. Chem. Phys.*, 15, 6023-6034, 10.5194/acp-15-6023-2015, 2015.

775 Jimenez, J., Canagaratna, M., Donahue, N., Prevot, A., Zhang, Q., Kroll, J., DeCarlo,
776 P., Allan, J., Coe, H., and Ng, N.: Evolution of organic aerosols in the atmosphere,
777 *Science*, 326, 1525-1529, 2009.

778 Li, W., Shao, L., and Buseck, P.: Haze types in Beijing and the influence of
779 agricultural biomass burning, *Atmos. Chem. Phys.*, 10, 8119-8130, 2010.

780 Li, Y., Schwab, J. J., and Demerjian, K. L.: Measurements of ambient ammonia using
781 a tunable diode laser absorption spectrometer: Characteristics of ambient ammonia
782 emissions in an urban area of New York City, *J. Geophys. Res.*, 111, D10S02,
783 10.1029/2005jd006275, 2006.

784 Li, Y., Lee, B., Su, L., Fung, J., and Chan, C.: Seasonal characteristics of fine
785 particulate matter (PM) based on high-resolution time-of-flight aerosol mass
786 spectrometric (HR-ToF-AMS) measurements at the HKUST Supersite in Hong
787 Kong, *Atmos. Chem. Phys.*, 15, 37-53, 2015.

788 Lu, Z., Zhang, Q., and Streets, D. G.: Sulfur dioxide and primary carbonaceous
789 aerosol emissions in China and India, 1996–2010, *Atmos. Chem. Phys.*, 11,
790 9839-9864, 10.5194/acp-11-9839-2011, 2011.

791 Matthew, B. M., Middlebrook, A. M., and Onasch, T. B.: Collection efficiencies in an
792 Aerodyne Aerosol Mass Spectrometer as a function of particle phase for laboratory
793 generated aerosols, *Aerosol Sci. Tech.*, 42, 884-898, 2008.

794 Meng, Z., Ding, G., Xu, X., Xu, X., Yu, H., and Wang, S.: Vertical distributions of SO
795 2 and NO 2 in the lower atmosphere in Beijing urban areas, China, *Sci. Total*
796 *Environ.*, 390, 456-465, 2008.

797 Meng, Z., Lin, W., Jiang, X., Yan, P., Wang, Y., Zhang, Y., Jia, X., and Yu, X.:
798 Characteristics of atmospheric ammonia over Beijing, China, *Atmos. Chem. Phys.*,
799 11, 6139-6151, 2011.

800 Middlebrook, A. M., Bahreini, R., Jimenez, J. L., and Canagaratna, M. R.: Evaluation
801 of composition-dependent collection efficiencies for the aerodyne aerosol mass
802 spectrometer using field data, *Aerosol Sci. Tech.*, 46, 258-271, 2012.

803 Mohr, C., Huffman, J. A., Cubison, M. J., Aiken, A. C., Docherty, K. S., Kimmel, J. R.,
804 Ulbrich, I. M., Hannigan, M., and Jimenez, J. L.: Characterization of primary
805 organic aerosol emissions from meat cooking, trash burning, and motor vehicles
806 with high-resolution aerosol mass spectrometry and comparison with ambient and
807 chamber observations, *Environ. Sci. Technol.*, 43, 2443-2449, 2009.

808 Ng, N. L., Herndon, S. C., Trimborn, A., Canagaratna, M. R., Croteau, P., Onasch, T.
809 B., Sueper, D., Worsnop, D. R., Zhang, Q., and Sun, Y.: An Aerosol Chemical
810 Speciation Monitor (ACSM) for routine monitoring of the composition and mass
811 concentrations of ambient aerosol, *Aerosol Sci. Tech.*, 45, 780-794, 2011.

812 Paatero, P., and Tapper, U.: Positive matrix factorization: A non - negative factor
813 model with optimal utilization of error estimates of data values, *Environmetrics*, 5,
814 111-126, 1994.

815 Parworth, C., Fast, J., Mei, F., Shippert, T., Sivaraman, C., Tilp, A., Watson, T., and
816 Zhang, Q.: Long-term measurements of submicrometer aerosol chemistry at the
817 Southern Great Plains (SGP) using an Aerosol Chemical Speciation Monitor
818 (ACSM), *Atmos. Environ.*, 106, 43-55, 2015.

819 Petit, J.-E., Favez, O., Sciare, J., Crenn, V., Sarda-Estève, R., Bonnaire, N., Močnik,
820 G., Dupont, J.-C., Haeffelin, M., and Leoz-Garziandia, E.: Two years of near
821 real-time chemical composition of submicron aerosols in the region of Paris using
822 an Aerosol Chemical Speciation Monitor (ACSM) and a multi-wavelength
823 Aethalometer, *Atmos. Chem. Phys.*, 15, 2985-3005, 2015.

824 Pope III, C. A., Ezzati, M., and Dockery, D. W.: Fine-particulate air pollution and life
825 expectancy in the United States, *New England Journal of Medicine*, 360, 376-386,
826 2009.

827 Quinn, P., Bates, T., Coffman, D., Onasch, T., Worsnop, D., Baynard, T., De Gouw, J.,
828 Goldan, P., Kuster, W., and Williams, E.: Impacts of sources and aging on
829 submicrometer aerosol properties in the marine boundary layer across the Gulf of
830 Maine, *J. Geophys. Res.: Atmos.* (1984–2012), 111, D23S36,
831 doi:10.1029/2006jd007582, 2006.

832 Sun, J., Zhang, Q., Canagaratna, M. R., Zhang, Y., Ng, N. L., Sun, Y., Jayne, J. T.,
833 Zhang, X., Zhang, X., and Worsnop, D. R.: Highly time- and size-resolved
834 characterization of submicron aerosol particles in Beijing using an Aerodyne

835 Aerosol Mass Spectrometer, *Atmos. Environ.*, 44, 131-140, 2010.

836 Sun, Y.-L., Zhang, Q., Schwab, J., Demerjian, K., Chen, W.-N., Bae, M.-S., Hung,
837 H.-M., Hogrefe, O., Frank, B., and Rattigan, O.: Characterization of the sources
838 and processes of organic and inorganic aerosols in New York city with a
839 high-resolution time-of-flight aerosol mass spectrometer, *Atmos. Chem. Phys.*, 11,
840 1581-1602, 2011.

841 Sun, Y., Zhuang, G., Tang, A., Wang, Y., and An, Z.: Chemical characteristics of PM_{2.5}
842 and PM₁₀ in haze-fog episodes in Beijing, *Environ. Sci. Technol.*, 40, 3148-3155,
843 2006.

844 Sun, Y., Wang, Y., and Zhang, C.: Measurement of the vertical profile of atmospheric
845 SO₂ during the heating period in Beijing on days of high air pollution, *Atmos.*
846 *Environ.*, 43, 468-472, 2009.

847 Sun, Y., Wang, Z., Dong, H., Yang, T., Li, J., Pan, X., Chen, P., and Jayne, J. T.:
848 Characterization of summer organic and inorganic aerosols in Beijing, China with
849 an Aerosol Chemical Speciation Monitor, *Atmos. Environ.*, 51, 250-259, 2012a.

850 Sun, Y., Zhang, Q., Schwab, J., Yang, T., Ng, N., and Demerjian, K.: Factor analysis
851 of combined organic and inorganic aerosol mass spectra from high resolution
852 aerosol mass spectrometer measurements, *Atmos. Chem. Phys.*, 12, 8537-8551,
853 2012b.

854 Sun, Y., Song, T., Tang, G., and Wang, Y.: The vertical distribution of PM_{2.5} and
855 boundary-layer structure during summer haze in Beijing, *Atmos. Environ.*, 74,
856 413-421, 2013a.

857 Sun, Y., Wang, Z., Fu, P., Jiang, Q., Yang, T., Li, J., and Ge, X.: The impact of relative
858 humidity on aerosol composition and evolution processes during wintertime in
859 Beijing, China, *Atmos. Environ.*, 77, 927-934, 2013b.

860 Sun, Y., Wang, Z., Fu, P., Yang, T., Jiang, Q., Dong, H., Li, J., and Jia, J.: Aerosol
861 composition, sources and processes during wintertime in Beijing, China, *Atmos.*
862 *Chem. Phys.*, 13, 4577-4592, 2013c.

863 Sun, Y., Jiang, Q., Wang, Z., Fu, P., Li, J., Yang, T., and Yin, Y.: Investigation of the
864 sources and evolution processes of severe haze pollution in Beijing in January
865 2013, *J. Geophys. Res.: Atmos.*, 119, 4380-4398, 2014.

866 Sun, Y., Du, W., Wang, Q., Zhang, Q., Chen, C., Chen, Y., Chen, Z., Fu, P., Wang, Z.,
867 Gao, Z., and Worsnop, D.: Real-Time Characterization of Aerosol Particle
868 Composition above the Urban Canopy in Beijing: Insights into the Interactions
869 between the Atmospheric Boundary Layer and Aerosol Chemistry, *Environmental*
870 *Science & Technology* (In submitted), 2015.

871 Ting, M., Yue-Si, W., Jie, J., Fang-Kun, W., and Mingxing, W.: The vertical
872 distributions of VOCs in the atmosphere of Beijing in autumn, *Sci. Total Environ.*,
873 390, 97-108, 2008.

874 Ulbrich, I., Canagaratna, M., Zhang, Q., Worsnop, D., and Jimenez, J.: Interpretation
875 of organic components from Positive Matrix Factorization of aerosol mass
876 spectrometric data, *Atmos. Chem. Phys.*, 9, 2891-2918, 2009.

877 Wang, Y., Zhang, Q., He, K., Zhang, Q., and Chai, L.: Sulfate-nitrate-ammonium
878 aerosols over China: response to 2000–2015 emission changes of sulfur dioxide,

879 nitrogen oxides, and ammonia, *Atmos. Chem. Phys.*, 13, 2635-2652,
880 10.5194/acp-13-2635-2013, 2013.

881 Xiao, R., Takegawa, N., Zheng, M., Kondo, Y., Miyazaki, Y., Miyakawa, T., Hu, M.,
882 Shao, M., Zeng, L., and Gong, Y.: Characterization and source apportionment of
883 submicron aerosol with aerosol mass spectrometer during the PRIDE-PRD 2006
884 campaign, *Atmos. Chem. Phys.*, 11, 6911-6929, 2011.

885 Xu, W., Sun, Y., Chen, C., Du, W., Han, T., Wang, Q., Fu, P., Wang, Z., Zhao, X., and
886 Zhou, L.: Aerosol composition, oxidative properties, and sources in Beijing: results
887 from the 2014 Asia-Pacific Economic Cooperation Summit study, *Atmos. Chem.*
888 ~~*Phys. Atmospheric Chemistry and Physics Discussions*~~*Discuss.*, 15, 23407-23455,
889 2015.

890 Zhang, J., Sun, Y., Liu, Z., Ji, D., Hu, B., Liu, Q., and Wang, Y.: Characterization of
891 submicron aerosols during a month of serious pollution in Beijing, 2013, *Atmos.*
892 *Chem. Phys.*, 14, 2887-2903, 2014.

893 Zhang, Q., Worsnop, D., Canagaratna, M., and Jimenez, J.: Hydrocarbon-like and
894 oxygenated organic aerosols in Pittsburgh: insights into sources and processes of
895 organic aerosols, *Atmos. Chem. Phys.*, 5, 3289-3311, 2005.

896 Zhang, Q., Jimenez, J. L., Worsnop, D. R., and Canagaratna, M.: A case study of
897 urban particle acidity and its effect on secondary organic aerosol, *Environ. Sci.*
898 *Technol.*, 41, 3213-3219, 2007a.

899 Zhang, Q., Streets, D. G., He, K., Wang, Y., Richter, A., Burrows, J. P., Uno, I., Jang,
900 C. J., Chen, D., Yao, Z., and Lei, Y.: NO_x emission trends for China, 1995-2004:
901 The view from the ground and the view from space, *J. Geophys. Res.*, 112, D22306,
902 10.1029/2007jd008684, 2007b.

903 Zhang, Q., Jimenez, J. L., Canagaratna, M. R., Ulbrich, I. M., Ng, N. L., Worsnop, D.
904 R., and Sun, Y.: Understanding atmospheric organic aerosols via factor analysis of
905 aerosol mass spectrometry: a review, *Anal. Bioanal. Chem.*, 401, 3045-3067, 2011.

906 Zhang, Q., and Tie, X.: High solubility of SO₂: evidence in an intensive fog event
907 measured in the NCP region, China, *Atmos. Chem. Phys. Discuss.*, 11, 2931-2947,
908 10.5194/acpd-11-2931-2011, 2011.

909 Zhang, Q., Meng, J., Quan, J., Gao, Y., Zhao, D., Chen, P., and He, H.: Impact of
910 aerosol composition on cloud condensation nuclei activity, *Atmos. Chem. Phys.*, 12,
911 3783-3790, 2012.

912 Zhang, W., Zhang, Y., Lv, Y., Li, K., and Li, Z.: Observation of atmospheric boundary
913 layer height by ground-based LiDAR during haze days, *Journal of Remote Sensing*,
914 17, 981-992, 2013.

915 Zhang, Y., Tang, L., Wang, Z., Yu, H., Sun, Y., Liu, D., Qin, W., Canonaco, F., Prévôt,
916 A., and Zhang, H.: Insights into characteristics, sources, and evolution of
917 submicron aerosols during harvest seasons in the Yangtze River delta region, China,
918 *Atmos. Chem. Phys.*, 15, 1331-1349, 2015.

919 Zhao, X., Zhao, P., Xu, J., Meng, W., Pu, W., Dong, F., He, D., and Shi, Q.: Analysis
920 of a winter regional haze event and its formation mechanism in the North China
921 Plain, *Atmos. Chem. Phys.*, 13, 5685-5696, 2013.

922

923 **Table 1.** Summary of average meteorological variables for different periods and the
 924 mass differences of aerosol species between ground site and 260 m (= ground – 260
 925 m).

	Before APEC				During APEC		
	Entire	Ep1	Ep2	Ep3	Entire	APEC1	APEC2
<i>Meteorological Variables</i>							
RH (%)	47.1	48.4	69.7	56.7	29.8	34.2	38.5
T (°C)	13.3	16.7	12.5	10.9	9.0	11.5	8.1
WS (m s ⁻¹)	4.0	3.4	2.3	2.3	4.9	3.8	3.1
<i>Mass Differences (μg m⁻³)</i>							
Org	0.7	0.3	4.5	-5.2	9.6	14.6	13.6
SO ₄ ²⁻	3.4	3.0	8.8	1.3	1.3	1.6	1.9
NO ₃ ⁻	4.3	4.5	10.9	0.8	0.7	1.0	1.0
NH ₄ ⁺	3.9	4.2	9.0	2.3	1.6	2.9	2.3
Cl ⁻	-0.1	0.0	-0.4	-0.2	1.0	1.7	1.5
NR-PM ₁	12.1	12.0	32.8	-1.1	14.1	21.8	20.2

926

927 **Figure captions:**

928

929 **Figure 1.** Evolution of vertical profiles of (a) wind speed (WS) and (b) wind direction
930 (WD) from the measurements of the Doppler wind lidar. The time series of NR-PM₁
931 (=Org + SO₄²⁻ + NO₃⁻ + NH₄⁺ + Cl⁻) is shown as the black line in (a). The shaded area
932 refers to the APEC period (same for following figures).

933 **Figure 2.** Time series of (a) *T*, (b) RH, (c) WS and WD, (d) NR-PM₁ species (Org,
934 SO₄²⁻, NO₃⁻, NH₄⁺, and Cl⁻), and (f) mass fraction of each species in NR-PM₁. Two
935 clean periods and five haze episodes are marked in Fig. 2d for further discussions.

936 The meteorological parameters in this figure were all from the tower measurements.

937 **Figure 3.** Time series of (a) sulfur oxidation ratio (SOR), (b) ratio of NO₃⁻/SO₄²⁻, and
938 (c) NR-PM₁. The SOR and NO₃⁻/SO₄²⁻ were color coded by RH.

939 **Figure 4.** (a) Mass spectra of HOA and OOA, (b) diurnal variations of the mass
940 concentration and mass fraction of HOA and OOA, (c) time series of HOA, OOA, and
941 inorganic species (SO₄²⁻, NO₃⁻, Cl⁻). The correlations of HOA and OOA with
942 inorganic specie are also shown in the figure.

943 **Figure 5.** Submicron aerosol composition as a function of NR-PM₁ mass loadings (a)
944 before APEC and (b) during APEC. The solide line shows the probability of NR-PM₁
945 mass.

946 **Figure 6.** Average chemical composition of NR-PM₁ before and during APEC, and
947 also that of five haze episodes and two clean events marked in Fig. 2.

948 **Figure 7.** Diurnal variations of meteorological variables (*T*, RH, WS, and WD),
949 NR-PM₁ species, and OA factors before and during APEC. The change rates during
950 APEC (= (Before APEC – APEC)/ Before APEC × 100) are also marked as light gray
951 in the figure.

952 ~~**Figure 8.** Correlations between measured NH₄⁺ and predicted NH₄⁺ (=18×~~
953 ~~(2×SO₄²⁻/96 + NO₃⁻/62 + Cl⁻/35.5)) before and during APEC. The inset plot shows~~
954 ~~the correlations of measured NH₄⁺ vs. predicted NH₄⁺ at the ground site.~~

955 **Figure 98.** Variations of NR-PM₁ species and OA factors as a function of (a) RH and
956 (b) WS before and during APEC. The RH and WS were from the tower measurements
957 at 280 m.

958 **Figure 109.** Wind rose plots (a) before APEC and (b) during APEC.

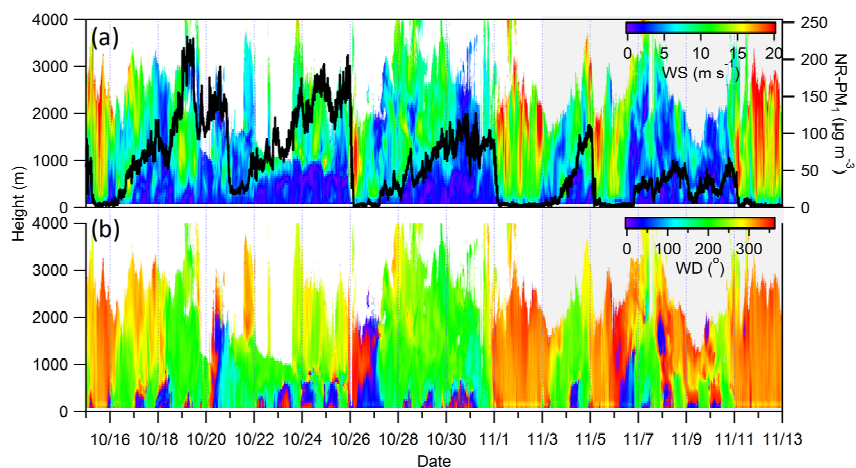
959 **Figure 110.** The average NR-PM₁ composition for each cluster (a) before and (b)
960 during APEC. The numbers on the pie charts refer to the average total NR-PM₁ mass
961 for each cluster. In addition, the number of trajectories and its percentage to the total
962 trajectories are also shown in the legends.

963 **Figure 1211.** Comparisons of time series of total NR-PM₁ mass and NR-PM₁ species
964 between 260 m and ground level.

965 **Figure 1312.** Average chemical composition of the difference between ground level
966 and 260 m (a) before APEC and (b) during APEC. The “1%” in the box indicates
967 lower concentration of chloride at ground site than 260 m.

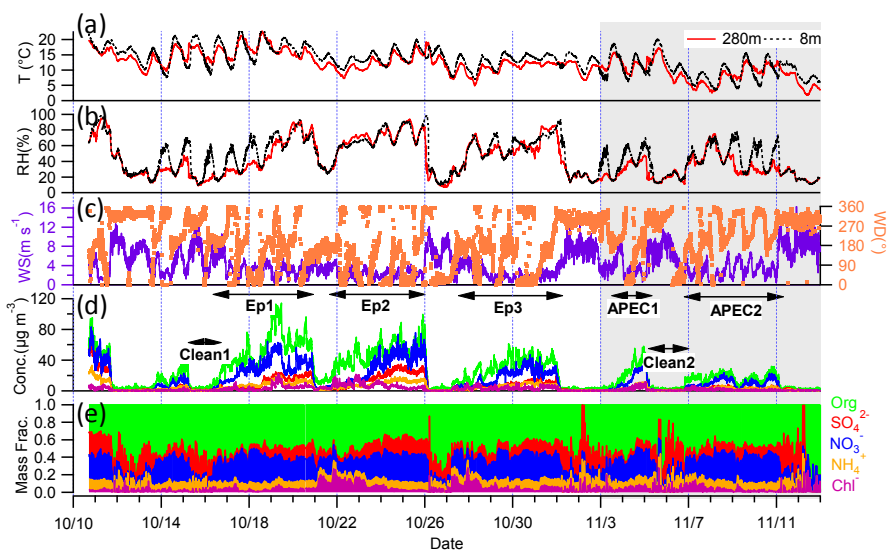
968 **Figure 1413.** The evolution of vertical profiles of meteorological variables (WD,
969 WS, RH, and *T*), and NR-PM₁ concentration at 260 m and ground site during two
970 pollution episodes (a) Ep2 and (b) APEC2. The vertical profiles of wind speed and

971 wind direction were from the measurements of the Doppler wind lidar, and those of
972 RH and T were from the tower measurements. The white areas in the figure indicate
973 that the data were not available.



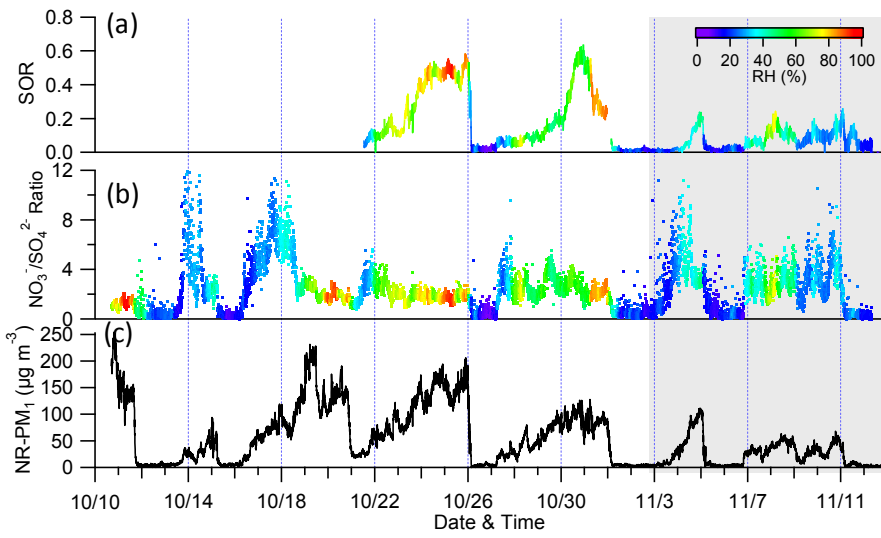
974

975 **Figure 1.** Evolution of vertical profiles of (a) wind speed (WS) and (b) wind direction
 976 (WD) from the measurements of the Doppler wind lidar. The time series of NR-PM₁
 977 (= Org + SO₄²⁻ + NO₃⁻ + NH₄⁺ + Cl⁻) is shown as the black line in (a). The shaded
 978 area refers to the Asia–Pacific Economic Cooperation (APEC) summit period, which
 979 is the same in the following figures.



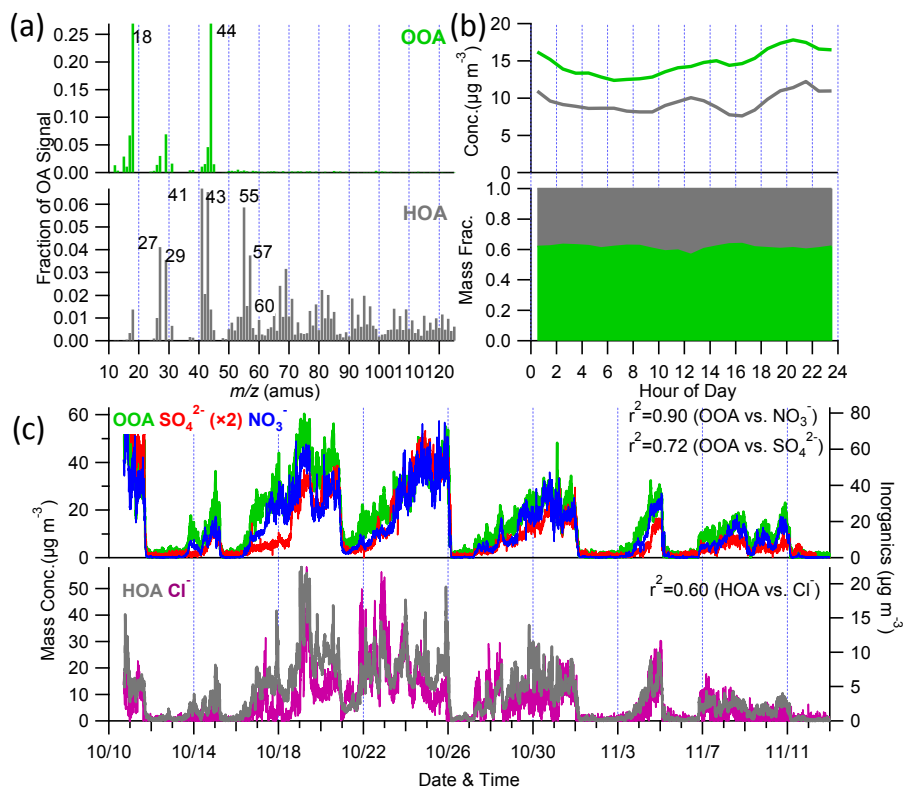
980

981 **Figure 2.** Time series of (a) temperature (T), (b) relative humidity (RH), (c) wind
 982 speed (WS) and wind direction (WD), (d) non-refractory submicron aerosol (NR-PM₁)
 983 species (Org, SO₄²⁻, NO₃⁻, NH₄⁺, and Cl⁻), and (e) mass fraction of each species in
 984 NR-PM₁. Two clean periods and five haze episodes are marked in Fig. 2d for further
 985 discussion. The meteorological parameters in this figure were all from the tower
 986 measurements.



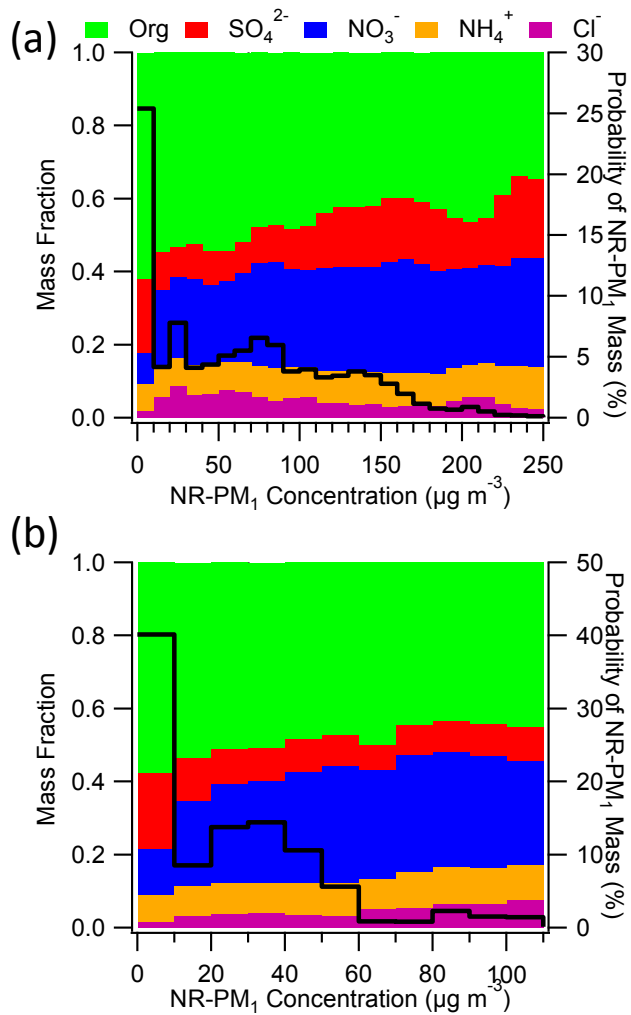
987

988 **Figure 3.** Time series of (a) sulfur oxidation ratio (SOR), (b) the ratio of $\text{NO}_3^-/\text{SO}_4^{2-}$,
 989 and (c) non-refractory submicron aerosol (NR-PM₁). The SOR and $\text{NO}_3^-/\text{SO}_4^{2-}$ are
 990 color coded by relative humidity (RH).



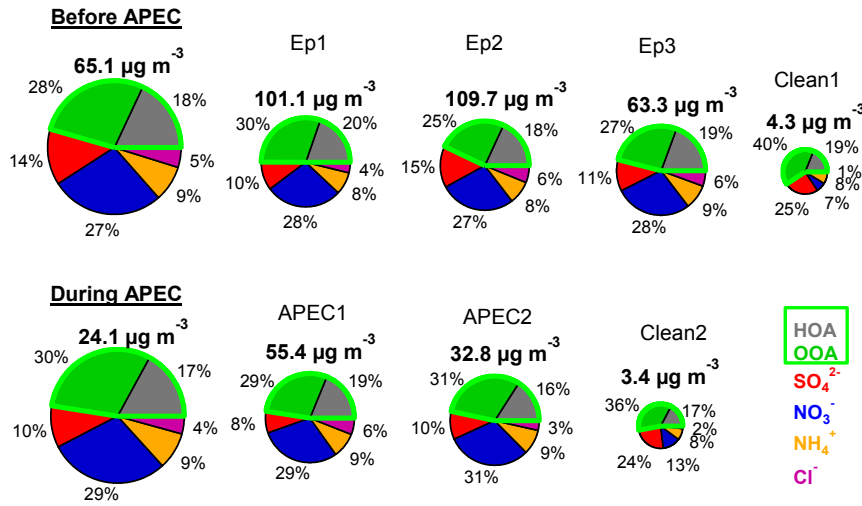
991

992 **Figure 4.** (a) Mass spectra of hydrocarbon-like organic aerosol (HOA) and
 993 oxygenated organic aerosol (OOA); (b) diurnal variations of the mass concentration
 994 and mass fraction of HOA and OOA; and (c) time series of HOA, OOA, and
 995 inorganic species (SO_4^{2-} , NO_3^- , Cl^-). The correlations of HOA and OOA with
 996 inorganic species are also shown in the figure.



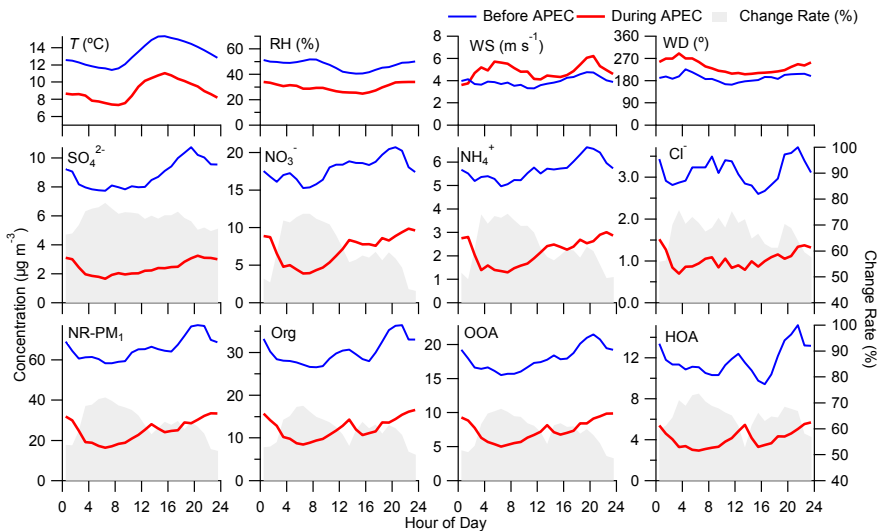
997

998 **Figure 5.** Submicron aerosol composition as a function of non-refractory submicron
 999 aerosol (NR-PM₁) mass loadings (a) before the Asia–Pacific Economic Cooperation
 1000 (APEC) summit and (b) during APEC. The solid line shows the probability of the
 1001 NR-PM₁ mass.



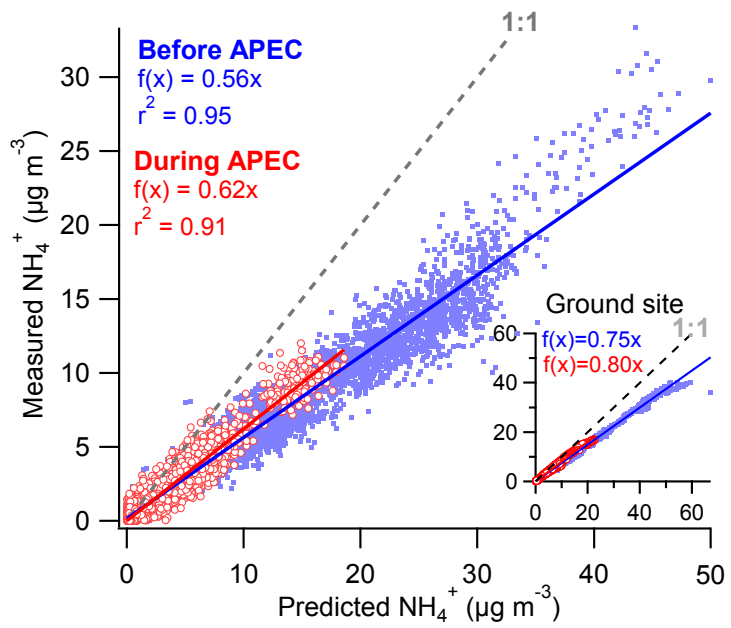
1002

1003 **Figure 6.** Average chemical composition of non-refractory submicron aerosol
 1004 (NR-PM₁) before and during the Asia-Pacific Economic Cooperation (APEC) summit
 1005 and that of five haze episodes and two clean events marked in Fig. 2.



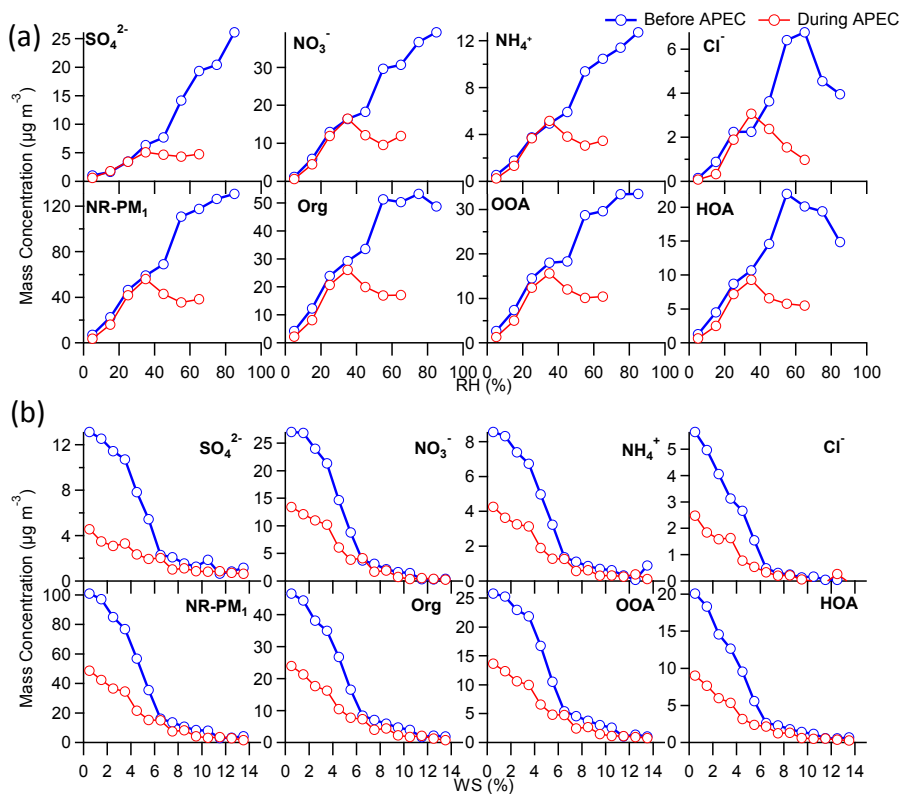
1006

1007 **Figure 7.** Diurnal variations of meteorological variables such as temperature (T),
 1008 relative humidity (RH), wind speed (WS), and wind direction (WD); non-refractory
 1009 submicron aerosol (NR-PM₁) species; and organic aerosol (OA) factors before and
 1010 during the Asia-Pacific Economic Cooperation (APEC) summit. The change rates
 1011 during APEC (= (Before APEC–APEC)/Before APEC \times 100) are also marked in light
 1012 gray in the figure.



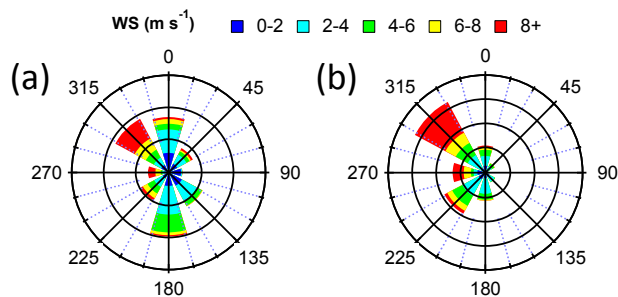
1013

1014 **Figure 8.** Correlations between measured NH_4^+ and predicted NH_4^+ ($= 18 \times (2 \times$
1015 $\text{SO}_4^{2-}/96 + \text{NO}_3^-/62 + \text{Cl}^-/35.5)$) before and during the Asia-Pacific Economic
1016 Cooperation (APEC) summit. The inset plot shows the correlations of measured NH_4^+
1017 versus predicted NH_4^+ at the ground site.



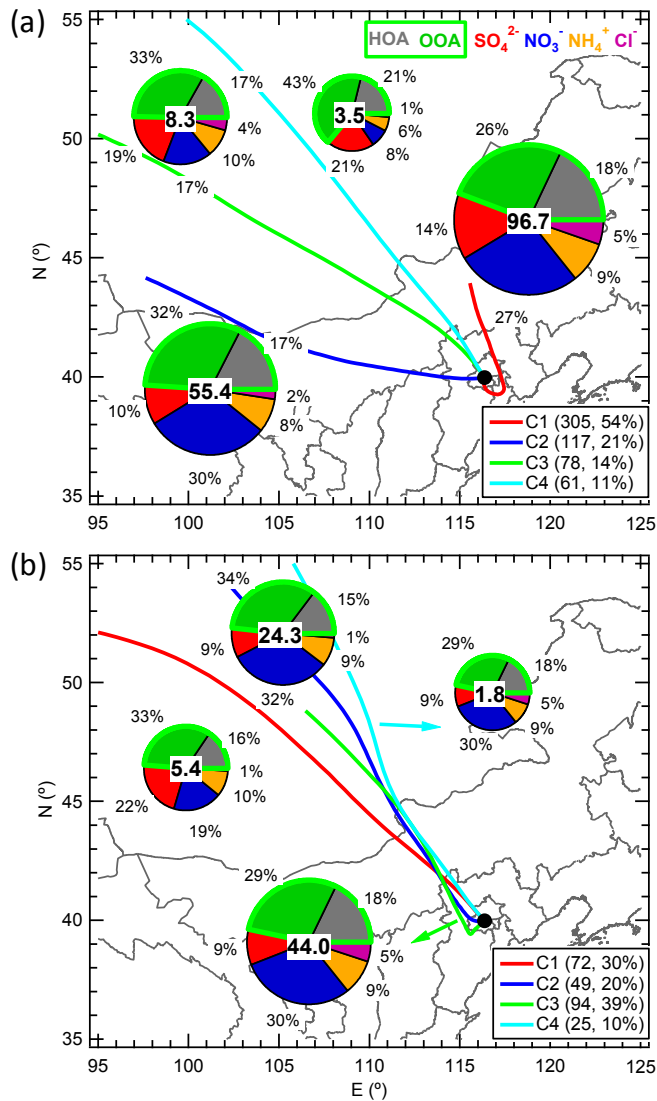
1018

1019 | **Figure 98.** Variations of non-refractory submicron aerosol (NR-PM₁) species and
 1020 organic aerosol (OA) factors as a function of (a) relative humidity (RH) and (b) wind
 1021 speed (WS) before and during the Asia-Pacific Economic Cooperation (APEC)
 1022 summit. The RH and WS were from the tower measurements at 280 m.



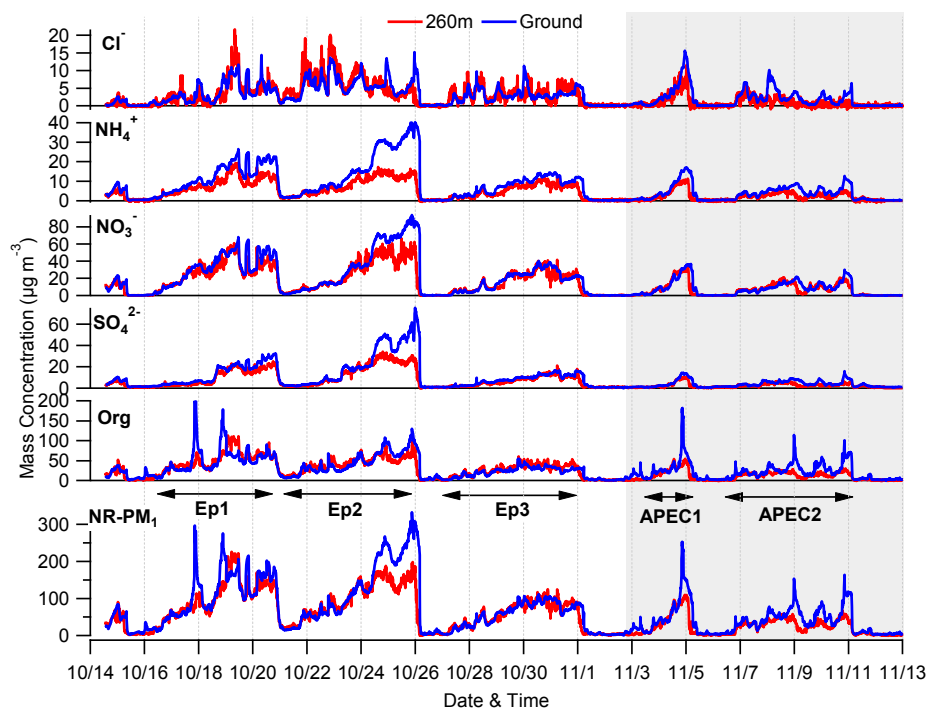
1023

1024 | **Figure 109.** Wind increase plots (a) before the Asia-Pacific Economic Cooperation
 1025 (APEC) summit and (b) during APEC.



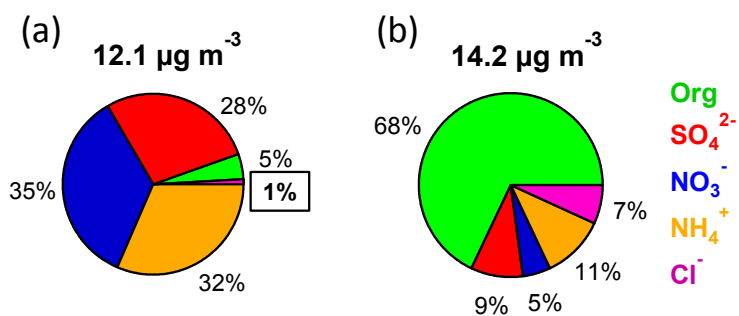
1026

1027 | **Figure 1110.** Average non-refractory submicron aerosol (NR-PM₁) composition for
 1028 each cluster (a) before and (b) during the Asia-Pacific Economic Cooperation (APEC)
 1029 summit. The numbers on the pie charts refer to the average total NR-PM₁ mass for
 1030 each cluster. In addition, the number of trajectories and its percentage to the total
 1031 trajectories are also shown in the legends.



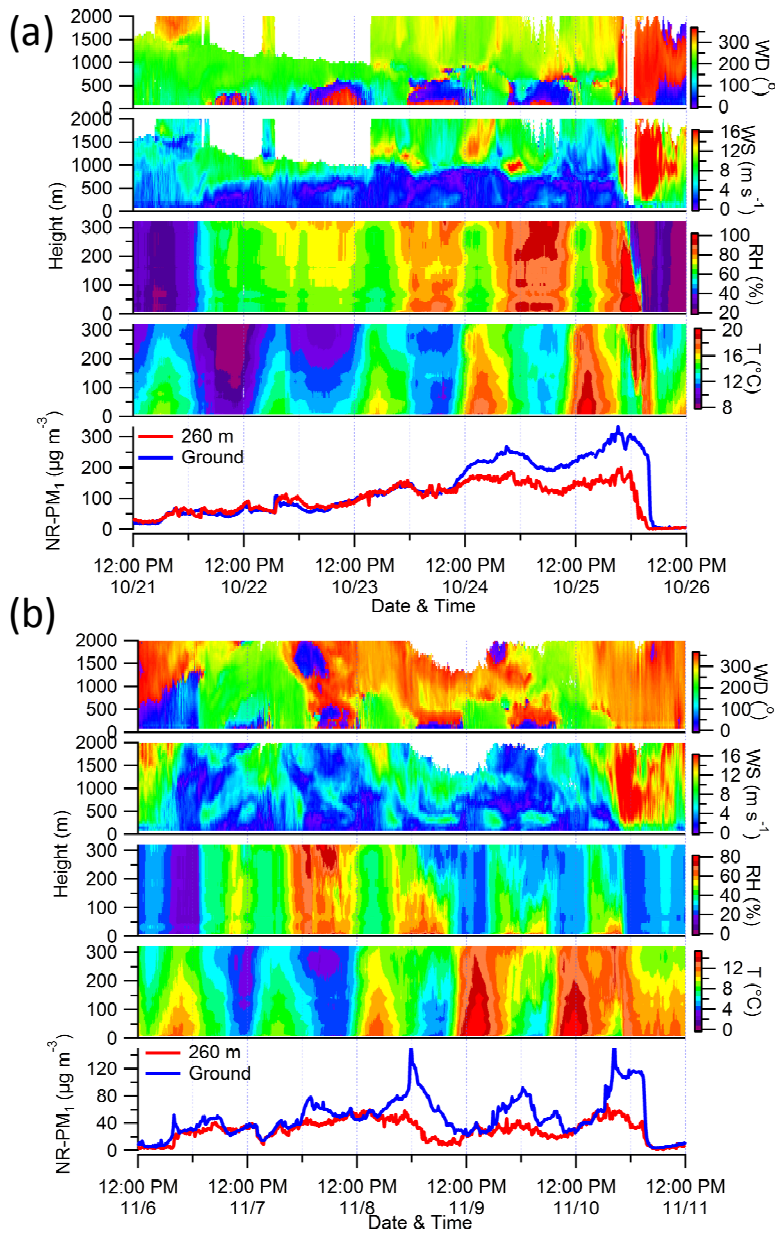
1032

1033 | **Figure 1211.** Comparisons of time series of total non-refractory submicron aerosol
 1034 (NR- PM_{10}) mass and NR- PM_{10} species between 260 m and the ground level.



1035

1036 | **Figure 1312.** Average chemical composition of the difference between ground level
 1037 and 260 m (a) before the Asia–Pacific Economic Cooperation (APEC) summit and (b)
 1038 during APEC. “1%” shown in the box indicates a lower concentration of chloride at
 1039 the ground site than that at 260 m.



1040

1041 | **Figure 1413.** Evolution of vertical profiles of meteorological variables such as wind
 1042 direction (WD), wind speed (WS), relative humidity (RH), and temperature (T) and
 1043 non-refractory submicron aerosol (NR-PM₁) concentration at 260 m and the ground
 1044 site during two pollution episodes (a) Ep2 and (b) APEC2. The vertical profiles of
 1045 wind speed and wind direction were from the measurements of the Doppler wind lidar,
 1046 and those of RH and T were from the tower measurements. The white areas in the
 1047 figure indicate that the data were not available.